The Design of a Molecular Assembly Line Based on Biological Molecules
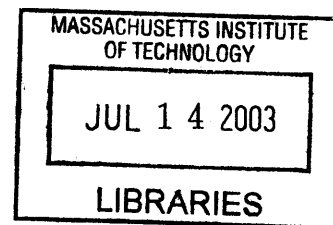
by

Brian Chow

B.S. Chemistry
Stanford University (2001)

Submitted to the Program in Media Arts and Sciences,
School of Architecture and Planning
in partial fulfillment of the requirements for the degree of
Master of Science in Media Arts and Sciences
at the
Massachusetts Institute of Technology
June 2003

Author _____

Program in Media Arts and Sciences
School of Architecture and Planning
May 22, 2003

Certified by _____

Joseph M. Jacobson
Associate Professor
Program in Media Arts and Sciences
School of Architecture and Planning

Accepted by _____

Andrew Lippman
Chairman, Departmental Committee on Graduate Students

ROTCH

The Design of a Molecular Assembly Line Based on Biological Molecules

by

Brian Chow

Submitted to the Program in Media Arts and Sciences,
School of Architecture and Planning
in partial fulfillment of the requirements for the degree of
Master of Science in Media Arts and Sciences
at the
Massachusetts Institute of Technology
June 2003

Abstract

A general scheme towards a "molecular assembly line" based on biological molecules is proposed, as well as its potential uses as a universal polymer scaffold in programmed assembly and molecular electronics. It is based on the principles of the biological molecules polyketide synthase and kinesin, and in some embodiments, may employ biomolecules like DNA as components of the system. The scheme entails the construction of a polymeric chain that moves a shuttle along the chain by controlling the interactions between the shuttle and individual monomer units using external inputs. The experimental work here particularly focuses on the design and synthesis of the monomer units and shuttles, as well as the mechanisms of control over the monomer/shuttle interactions that are required to construct the proposed polymer systems. Two approaches are explored, the first of which utilizes radio-frequency magnetic fields to selectively dehybridize DNA by coupling RF to covalently attached nanoparticle antennae. The second approach utilizes wavelength selective photocleavage of carbonyl bonds to control the equilibrium of a Michael reaction, and will demonstrate how one can construct a purely synthetic analogue of a polyketide synthase.

Thesis Supervisor:
Joseph M. Jacobson
Associate Professor
Program in Media Arts and Sciences
School of Architecture and Planning

The Design of a Molecular Assembly Line Based on Biological Molecules

by

Brian Chow

Thesis Committee
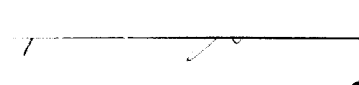
Thesis supervisor _____

Joseph M. Jacobson
Associate Professor
Program in Media Arts and Sciences
School of Architecture and Planning

Thesis reader _____

Shuguang Zhang
Associate Director
Center for Biomedical Engineering

Thesis reader _____

Robert C. O'Handley
Senior Research Scientist
Department of Materials Science and Engineering

"A chemist comes to us and says, 'Look, I want a molecule that has the atoms arranged thus and so; make me that molecule.' The chemist does a mysterious thing when he wants to make a molecule. He sees that it has got that ring, so he mixes this and that, and he shakes it, and he fiddles around. And, at the end of a difficult process, he usually does succeed in synthesizing what he wants. By the time I get my devices working, so that we can do it by physics, he will have figured out how to synthesize absolutely anything, so that this will really be useless."

- Richard P. Feynman, "There's Plenty of Room at the Bottom" (1959)

Table of Contents

Chapter 1: Introduction

1.0 – Overview

This thesis discusses the general design of a "molecular assembly line" based on biological molecules for the purpose of programmed assembly at the molecular level. The molecular assembly line is a linear polymer chain that is a scaffold capable of passing a solid support for chemical synthesis along the scaffold by any arbitrary pathway. The scheme is based on biological molecules in that it is based on the principles of biology's robust assembly processes, and also in that various embodiments of the assembly line may employ biological molecules as building blocks. In addition to outlining a general scheme, this thesis will also present experimental results on some basic building blocks of different types of molecular assembly lines.

Why would one want to create a molecular assembly line? The notion that thousands of "tiny hands" could work in parallel to construct devices by maneuvering individual atoms was first proposed over 40 years ago by Richard Feynman in his prophetic speech - "There's Plenty of Room at the Bottom" [Feynman59]. The dream was realized in 1993, when IBM researchers [Eigler93] arranged xenon atoms into the IBM logo by using a scanning tunneling microscope (STM) tip to pick-and-place individual xenon atoms on a nickel surface (figure1.1.). After this tour de force, the notion that humans could build complex systems atom by atom no longer seemed like a pipe dream.

"What would the properties of materials be if we could really arrange the atoms the way we want them? They would be very interesting to investigate theoretically. I can't see exactly what would happen, but I can hardly doubt that when we have some *control* of the arrangement of things on a small scale we will get an enormously greater range of possible properties that substances can have, and of different things that we can do."

- Richard P. Feynman, (1959)
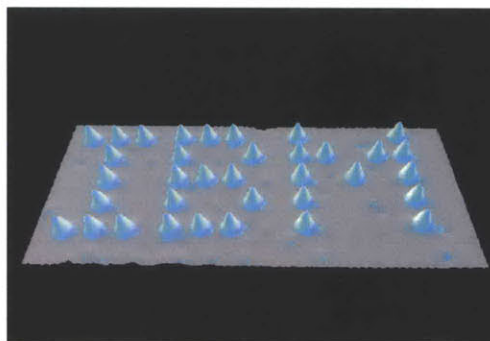
Figure 1.1 Xenon atoms arranged into the IBM logo on a nickel surface using a STM tip. Image from [Eigler93]

In recent years, largely driven by the desire to construct physical systems with 2-D assembly and 3-D folding rules like proteins, researchers have been working towards

programmed assembly [Whitesides02], in which various structures can be created from a universal parts set. The notion of *programmable chemistry* [Lehn00][Stoddart02], the synthesis of various chemicals from universal precursors, has also become popular recently. In these programmable systems, the outcome of the assembly or synthesis depends on the inputs into the system, usually chemical, electrical, or optical. *Molecular electronics* have also come to prominence in recent years for the vast potential device density and higher performance in devices utilizing quantum size effects. Indeed, if an individual molecule could be used as a switch, one liter of a 1M solution could potentially hold on the order of 10^{23} switches, or roughly 10^{11} Pentium IV chips, which contain about one trillion elements.

The proposed molecular assembly line will be important to these fields because it represents a system that is truly molecular, scaleable, and programmable. As will be discussed in section 1.1, even though many molecular devices have been demonstrated, these devices often contain only one component that is a molecule, and the rest is lithographically defined on a 2-D surface; the device is more "molecule-based" than "truly molecular" in nature. Truly molecular devices have been shown, but it has yet to be shown how these systems can be built-up. The molecular assembly line will demonstrate how to construct analogs to scaleable and robust biological systems, and it will shed light on how biological molecules can be used for general computational purposes, like the construction of bi-stable molecular switches.

In this chapter, section 1.1 overviews the current state of molecular devices and some of the issues surrounding devices that have been reported in the literature. Section 1.2 describes the biological inspirations for the proposed molecular assembly line. Section 1.3 proposes the general scheme of the molecular assembly line and various embodiments of the system.

Chapter 2 proposes a molecular assembly line based on "RF Biology" – the control of DNA hybridization states by coupling radio-frequency magnetic fields into covalently attached superparamagnetic nanoparticle antennae. Chapter 3 proposes an alternative mechanism of controlling biological molecules using static magnetic fields, termed "DC Biology." Chapter 4 proposes a molecular assembly line based on wavelength selective

photocleavage of carbonyl compounds. Finally, chapter 5 summarizes the work presented.

1.1 – Issues in molecular devices

In recent years, nanotechnology research has come to significant prominence, but the term is broad and ill defined. Likewise, many terms used in discussing nanotechnology are also ill defined, terms as simple as "molecular." For example, is a Pentium IV, which currently has a design rule of 110nm, considered "nanotechnology?" Before discussing the merits of and problems with molecular devices, certain *arbitrary* definitions or requirements must be made to limit the scope of this introduction and thesis.

The size benefits of devices in nanotechnology - will be limited to device density. Ballistic transport, electron tunneling, quantum entanglement, and other physical phenomena associated with the nanometer size scale will not be considered, despite their importance in nanotechnology with respect to computational speed, efficiency, energy consumption, and cryptography.

For a device to be considered "molecular" - the device must be built by a bottom-up approach; the device cannot be created in its entirety by lithography or any other top-down approach, even if every component is in the nanometer size scale. This rules out Pentiums and other purely lithographically defined devices that have design rules in the nanometer regime.

For a device to be considered "truly molecular" – the entire device must be soluble in some solvent after fabrication. The presence of a 2-D surface or substrate must not be absolutely necessary to its performance. This rules out a process like manipulating atoms with a STM tip as shown in figure 1.1.

The term "programmable" - entails the ability to affect the system such that there is only one outcome despite there being many potential outcomes initially.

The term "externally programmable" - requires a remote input that does not require spatial confinement to address the system elements. Once again, this rules out a Pentium chip that requires wire bonding between lithographically defined electrode structures, or a process like manipulating atoms with a STM tip.

How "scaleable" a device is – is a matter of how large or complex of a system can be built by only adding individual devices to the system being constructed. For example, the ability to construct logic gates out of switching elements is the measure of how scaleable the switch is, but the ability to build processors out of the logic gates does not reflect on the scaleability of the switches. This limitation must be made because the connecting of many higher-order devices does require spatial confinement in almost all schemes proposed in molecular electronics, including externally programmable systems.

It would be impossible to summarize and discuss all molecular machines and devices that have ever been constructed, but here they are put in two categories, molecule-based devices employing lithography, or unscaleable molecular systems in solution.

1.1.1 – Molecule-based devices employing lithography

In recent years, many researchers have been using nanotubes, nanowires, nanoparticles, polymers, and individual molecules to build nanoscale devices like field-effect transistors [Avouris01] by replacing the lithographically defined semi-conductor gap with semi-conducting molecular components (figure 1.2). While there are exciting phenomena associated with this size scale, in particular, tunneling [McEuen96], ballistic transport [Dai01], and quantum entanglement [Herz02], nearly zero Kelvin (liquid helium) temperatures are typically required for these devices to utilize these phenomena.
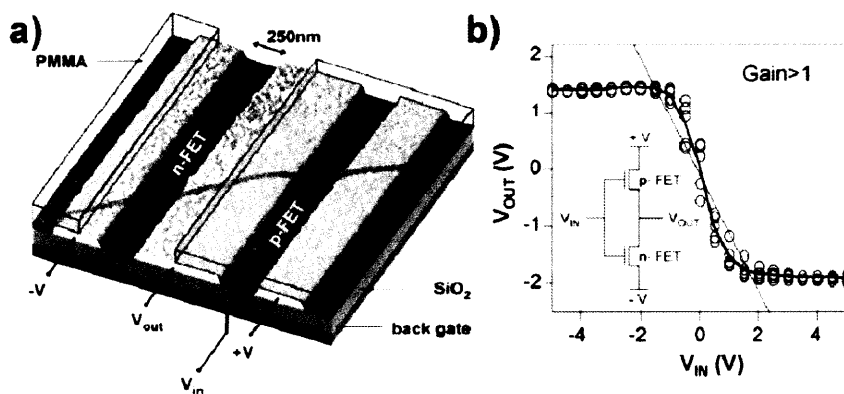
Figure 1.2 Not-gate (inverter) composed of a semi-conducting single-walled carbon nanotube bridging two sets of electrodes. A thick layer of PMMA resist covers part of the nanotube (naturally p-type) nanotube prior to chemical doping. Image from [Avouris01].

At room temperature at which thermal noise washes out these size-induced effects, there is limited size benefit in replacing a traditional semi-conductor junction with a

molecular component because the device size is ultimately limited by the size of the lithographically defined features. If one reduces the size of the head of a hammer but not the handle size, one is not left with a smaller hammer, but rather a disproportioned one. A similar argument can be made against the expectations that replacing bulk crystalline silicon with molecular components will automatically lead to major device miniaturization. However, if each molecular component in the device is an independent and functional device, and externally/remotely addressable, the device density greatly increases.

1.1.2 – Unscaleable molecular devices in solution

Another route towards molecular machines and electronic devices is through purely supramolecular chemical syntheses of switching elements like rotaxanes and catenanes (figure 1.3) [Stoddart01] that switch their structure upon global oxidation/reduction. While these compounds are often amazing feats in chemical synthesis, their utility as functional devices is extremely limited by the fact that they are not scaleable in solution.
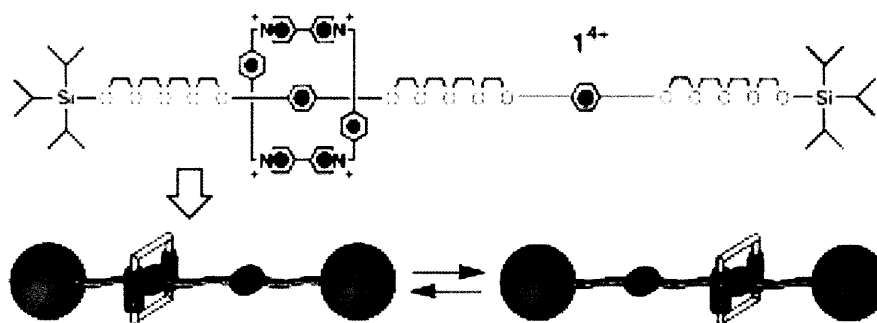
Figure 1.3 In the ([2]rotaxane 1^{4+}), the bipyridinium-based cyclophane shuttles from one 1,4-dioxybenzene recognition site to the other depending on the pH of the solution (oxidation / reduction state of the system). Image from [Stoddart01].

Azo compounds that undergo optically driven cis-trans isomerizations are also popular molecular switches [Petty95]. Artificial oligonucleotides have been synthesized with azo-benzene compounds at the 2' position that can be used to ratchet apart the strands in the DNA double helix by creating steric crowding upon cis-trans isomerization in the presence of UV light [Komiyama99]. Others have optically controlled phenylalanine-cyclodextrin host-guest interactions by blocking and unblocking the cyclodextrin host site with a covalently bound azo compound [Petty95]. These types of switches may lead to

interesting molecular machines, but they are volatile (with respect to memory), not bi-stable. Furthermore, the number of states that an azo switch can adopt is limited to two.

1.2 – Biological inspiration

As so aptly observed by Feynman [Feynman59], the "marvelous biological system" exhibits a staggering level of complexity that far exceeds the complexity of artificial systems at that size scale:

> The biological example of writing information on a small scale has inspired me to think of something that should be possible. Biology is not simply writing information; it is *doing something* about it. A biological system can be exceedingly small. Many of the cells are very tiny, but they are very active; they manufacture various substances; they walk around; they wiggle; and they do all kinds of marvelous things---all on a very small scale. Also, they store information. Consider the possibility that we too can make a thing very small, which does what we want---that we can manufacture an object that maneuvers at that level!

Let us look at DNA replication as an example. DNA polymerase is an enzyme roughly 10nm in diameter that is responsible for replicating DNA from a template strand. What can this biological machine do at 1/10 the size of a single line, which is not even a functional transistor, in the current state-of-the-art Pentium processor? ... It replicates at approximately 1000 base pairs per second with an error rate of one part per million [Carlson02]. This is absolutely remarkable.

It is extremely important to analyze the blueprints of biology or even consider the use of robust biological molecules as the building blocks when constructing molecular systems. Indeed, this is a trend becoming prevalent in many fields [DOE02], such as (but certainly not limited to) materials synthesis [Belcher00], computation [Winfree96], and control theory [Doyle02].

1.2.1 – Bio-inspired assemblers in the literature

Let us consider an assembler any system that can move a physical object along a linear chain. There are very few examples of assemblers in the literature, and ironically, *they too are based on biological principles or are built out of biological components.* The rotoxanes and catenanes mentioned previously have been called "molecular shuttles" for their ability to shuttle a molecule between two oxidation-reduction centers. These systems are largely based on the principles of metal ion coordination at biological redox centers.

There are two systems that require a 2-D substrate that are especially worth mentioning in the context of molecular assembly lines, even if they are not truly molecular by our definition. In the first system, Hopfield *et al.*, using Photosystems I and II as an inspiration, proposed an electronic shift register memory that passes electrons down a polymeric chain by photo-induced electron transfer reactions [Hopfield89]. In figure 1.4a, a laser pulse excites an electron to from the ground state of α, and then the electron decays to the ground states of β and γ, finally ending up in the ground state of the next α unit. The polymer is placed between two electrodes and bits are written by applying a large potential, thereby reducing the first α unit of the polymer. The bit is read at the drain electrode (figure 1.4b). This system is particularly important because it first introduced the notion that an object can be moved down a linear chain by pulsing a remote input. The molecular assembly line proposed in this thesis is based on this notion, as well as Hopfield's design of a polymerized chain of repeating α-β-γ units.

a)   b)
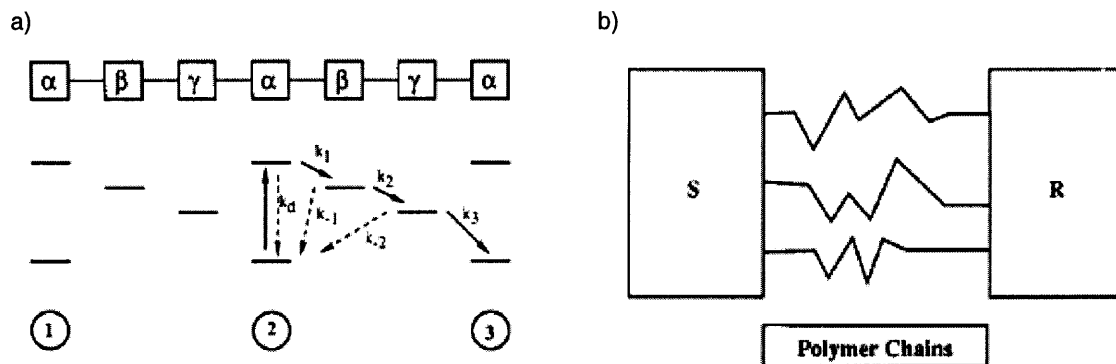
Figure 1.4 Electron energy level diagram for the Hopfield shift register. Electrons are excited by a UV pulse from the ground state to an excited state of an α_N unit and cascade down a polymer chain to the α_{N+1} unit via intermediate energy states, the ground states β and γ. **b)** Schematic design for reading and writing the bits. Bits are written by reducing the first α-units in the polymer chain at the source electrode (S), and read at the drain electrode (D). Images from [Hopfield89].

In the second system, Vogel *et al.* [Vogel01] moved a fluorescent microtubule along a substrate of patterned kinesin motor proteins (figure 1.5). When ATP is provided, the kinesin proteins push the microtubule along the surface. The microtubule transports streptavidin-coated beads that are bound to the microtubule via binding with biotin molecules that coat the microtubule surface. The motion can also be controlled remotely by first caging the ATP molecules, and then releasing them from the cages with UV irradiation; this provides a burst in energy source and initiates the microtubule

movement. The motion stops when all the ATP is consumed (figure 1.5b). Figure 1.5c shows the displacement of the microtubule after 40 seconds; the arrows point to bound streptavidin beads as a reference for measuring the displacement. As will be discussed in section 1.2.3, this is the opposite of what happens in biology; typically, the microtubule is static, and the kinesin moves along the microtubule track.
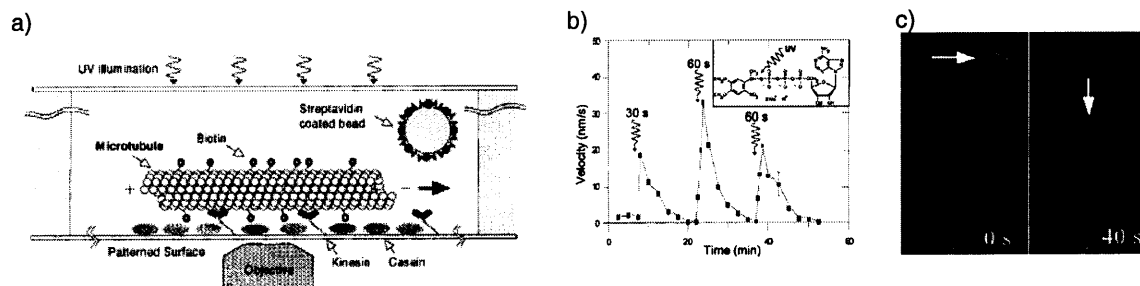
Figure 1.5 a) A microtubule shuttle carries a streptavidin bead along a kinesin surface. **b)** The velocity of the movement versus time. UV pulses every 30 seconds release caged-ATP molecules and initiate the microtubule movement by providing a burst of the energy source. **c)** Fluorescence images of the movement after 40 seconds. The arrows point to streptavidin coated beads ("cargo") as a reference for displacement. Images from [Vogel01].

1.2.2 – Polyketide synthase and covalent hand-off

The polyketide synthase (PKS), often referred to as "Nature's assembly line," is an enzyme found in plants that produces a class of antibiotics known as polyketides. A typical polyketide synthase can synthesize very large molecules with stereoselectivity at rates on the order of $pmol_{PK}$ / (minute $*$ μM_{PKS}) [Simpson98], which corresponds roughly to one perfect drug every 10 minutes per polyketide synthase from start to finish. This is an astounding rate, on the order of 10^4 times faster than commercial drug synthesis, if one assumes it takes the pharmaceutical industry somewhere between one week and one year to synthesize molecules of similar complexity and stereoselectivity (up to roughly 10 stereoselective centers) with any reasonable yield, not including the R&D and process development time.

Figure 1.6 shows how a polyketide synthase performs its molecular assembly process. The left image delineates the assembly line model of a PKS. A linear chain is synthesized, with the addition of a two-carbon unit, known as a ketide, per reaction step. Each ketide addition occurs in a separate "module" of the PKS, and the molecule is handed-off to the next module. Each module has a minimum of three monomeric enzymes, or "domains," that are polymerized - ketosynthase (KS), chain length factor

(CLF), and acyl carrier protein (ACP). In the figure, 6-deoxyerythronolide (6-DEB) is synthesized linearly and then cyclized. The cyclized 6-DEB can then serve as a precursor that can be tailored into several antibiotics, in this case erythromycin A [Hopwood97].
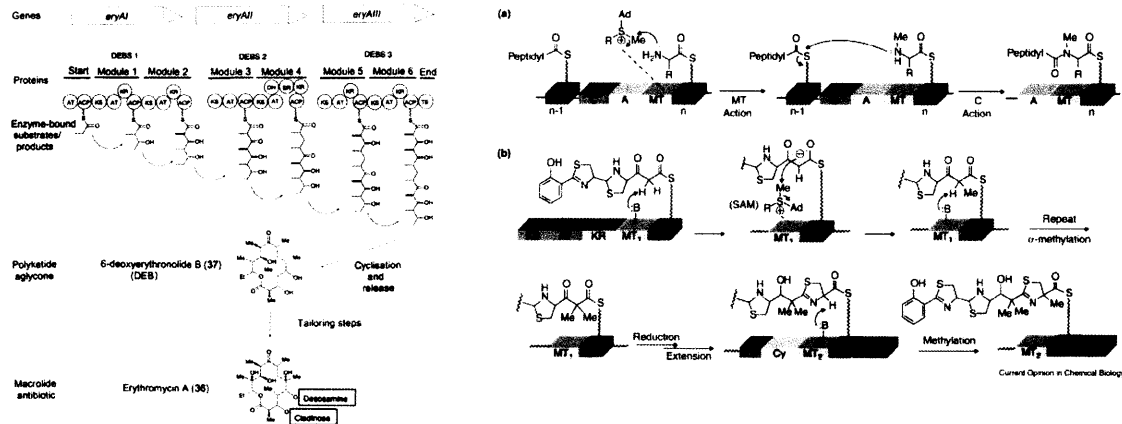
Figure 1.6 The polyketide synthase *left)* Assembly-line model polyketide synthases (PKS). 6-deoxyerythronolide (6-DEB) is synthesized linearly, and then cyclized. The 6-DEB precursor can be tailored into several antibiotics, in this case erythromycin A. Image from [Hopwood97]. *right)* Methylation of nonribosomal peptides by methyl transferase domains in polyketide synthases, showing how the enzyme performs covalent hand-off of small molecules between domains. Image from [Walsh01].

In the right image in figure 1.6, part "a" shows the working mechanism of covalent hand-off between subunits during the methylation of nonribosomal peptides by methyl transferase domains. First, an aminoacyl thioester is catalytically methylated by the coordination of S-adenosyl methionine and the thioester by the methyl transferase (MT) and PCP domains in the n-module. The now methylated aminoacyl thioester forms an amide bond with the peptidyl chain located at the PCP domain in the (n-1)-module, and the entire peptidyl chain is handed-off to the n-module because the amide bond strength is greater than the thioester bond.

So, how can the polyketide synthase accomplish the incredible feat of assembling complex structures with extreme speed and accuracy? First, every reactive step is catalyzed. Second, it achieves stereoselectivity by coordinating the orientation of the polyketide chain within the pockets of the enzyme as it is being synthesized. Third, it performs covalent hand-off of the molecule as it is being synthesized. This essentially eliminates diffusion in the synthesis process thereby shortening the reaction time. It also contributes to the stereoselectivity of the reaction because it guarantees that the

molecules are constrained in a certain manner when they are handed-off between the pockets in the enzyme. The hand-off also serves as a feedback mechanism for the reaction completion because the molecule cannot be handed-off between sites without the reaction occurring. Therefore, in examining Nature's assembly line, the following notion is key towards the design of a molecular assembly line:

In order to assemble something quickly and efficiently, diffusion must be eliminated by physically handing-off the object that is being assembled.

1.2.3 – Kinesin and the tethered walk

Kinesin (figure 1.7) is a motor protein that moves like a train on a filamentous microtubule track. Kinesin has several functions, like active intracellular transport of small molecules [Brady92] and stretching cells during cell division [Sharp00]. While it was originally believed that kinesin moves in only one direction like most motor proteins, from the net negative end to the positive end of the (electric) dipolar filament, it has now been shown that kinesin can move bi-directionally [Endow99].

The kinesin protein is a "two-head" protein, meaning it contains two motor regions that are bound to the microtubule track when it is not in motion. However, the "two-head" model does not preclude the possibility that only one of the heads is bound as kinesin moves along the filament; it has been shown that this is indeed the case [Vale00]. As can be seen in figure 1.7, when the protein is not in motion, both heads are bound to the filament. When the kinesin molecule moves, one head remains bound as the other head steps to the next binding site along the track. This is effectively a "tethered-walk," and while it is not termed as such in the literature, it will be called a tethered-walk from here on out. The bias in direction (net forward motion) during the "power-stroke" comes from conformational changes induced by ATP binding at the neck between the two heads, or in other words, the head-filament interaction drives the direction of movement.

This walk is fundamentally different from two-head motor proteins like myosin in which only one is head bound at any time and the heads are independent of one another. The directional movement in myosin during the power-stroke comes from the angular rotation of its long and tilted swivel arm as ATP binds to the arm. Myosin effectively skips along

the filament. One head dissociates as the other finds another binding site, but the system is not tethered.

a)

b)
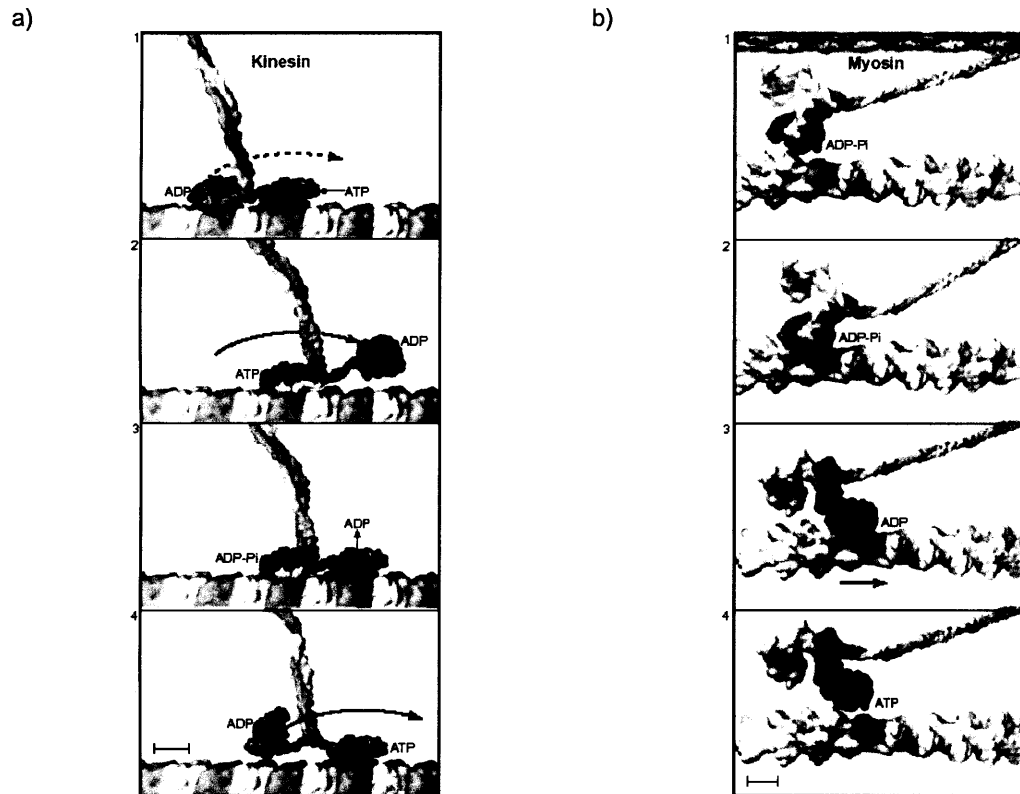
Figure 1.7 a) Tethered-walk in kinesin. One head is bound to the filamentous track, as the second head steps to the next binding-site on the track. **b)** Untethered hop in myosin in which both heads dissociate from the track as the protein moves between binding sites. Image from [Vale00].

Where does the action occur that confers directional movement in these systems? Directionality is conferred in kinesin from action that occurs between the motor heads and the filament, whereas in myosin, directionality is conferred by action in the arm and away from the filament as the entire system is dissociated. Therefore, in the context of the molecular assembly line that is being proposed (see section 1.3), kinesin movements show that:

In order to move an object along a polymer chain without dissociating the object from the polymer, a tethered-walk is required and one must control the interaction between the object and the polymer scaffold.

1.2.4 – Further discussion on biological assembly

Polyketide synthases and kinesins were discussed in great detail because of their relevance to the design of the molecular assembly line proposed in this thesis. But, let us take a brief moment to discuss more general lessons that biological systems can teach us about the requirements for quickly assembling complex structures with extreme precision at the molecular scale.

First, the assembly should be predicated. The polyketide synthase can quickly synthesize complex antibiotics because it covalently hands-off small molecules and because each step is catalyzed. It has this ability because the assembly is predicated, which allows the structure of the enzyme to be optimized for this process. Essentially, predication is required for the optimization of the kinetics and thermodynamics of a system. Once the system is optimized, it can be evolved with precise changes. Second, feedback is required. DNA polymerase can replicate DNA with incredible speed and fidelity because it has feedback mechanisms; polymerase not only uses the template strand to direct the assembly of the growing nucleotide chain, but also checks the added nucleotide against the template strand after the addition [Glick98]. Lastly, error-correcting codes are required. Perhaps biology's greatest example of error-correction is the *Deinococcus radiodurans*, an extremophilic bacterium capable of surviving incredibly extreme x-ray irradiation because it can salvage the damaged DNA strands and enzymatically reconstruct its entire genome in hours [Narumi00].

1.3 – The design of the molecular assembly line

There is no definition for a "molecular assembly line" in the literature, but in this thesis, it is defined as a system that meets the following requirements:

1) A polymer chain composed of monomers or "antennae."
2) *a.* A molecular "shuttle" (e.g. an individual molecule or nanoparticle) can be moved from one arbitrary monomer position along the polymer chain to any other monomer position for the purpose of assembling some chemical moiety onto the shuttle.
   b. The shuttle can move between these positions along any arbitrary pathway determined by a programmed set of inputs. Therefore, the movement must be bi-directional and reversible.
3) The inputs into the system that move the shuttle along the assembly line must be external.
4) For the system to be truly molecular, it must be soluble in some solvent

1.3.1 – Scheme

The general scheme for a molecular assembly line is shown in figure 1.8. The molecular assembly line is comprised of a polymer with a repeating pattern of 3 concatenated monomers or antennae, $-(1\text{-}2\text{-}3)_n\text{-}$. The repeating patter is shown in parenthesis in the figure. The yellow circle in the figure represents the shuttle. In the absence of any inputs, the shuttle has an equal binding affinity towards any of the antennae. Each input frequency effectively "turns off" attractive intermolecular forces between the respective antenna and the shuttle (i.e. $h\nu_1$ turns off the bond between the shuttle and antenna 1).

Assume that the shuttle is in position *a*, tethered between antennae 1 and 2 of the first (1-2-3) pattern (top). In order to move the shuttle from position *a* to position *b*, $h\nu_1$ is input, thereby preventing binding of the shuttle to any antenna 1. Because the shuttle is tethered to antenna 2 of this first pattern, it will be biased to toggle over to position *b*, between antennae 2 and 3 of the first pattern. Each time the bond between the shuttle and antenna 1 is reformed, it is broken again, but once a bond between the shuttle and antenna 3 is formed, the shuttle is in a stable position. This system is bi-directional and reversible; the shuttle can be toggled back to position *a* by inputting $h\nu_1$, or to position *c*

by inputting hv_2. The system has performed a tethered-walk. If the original position of the shuttle is known, it can be moved to any position along the molecular assembly line by any arbitrary pathway, given the correct input sequence. Therefore, the system is externally programmable.
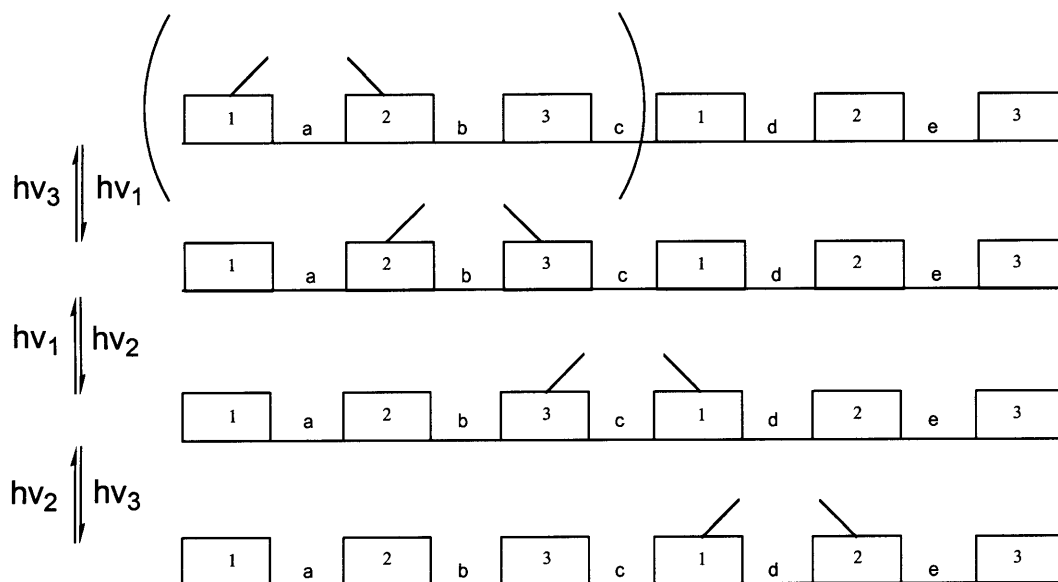
Figure 1.8 General scheme for a molecular assembly line. The circle represents a shuttle, and each rectangle represents a different antenna. The repeating pattern is shown in parentheses.

1.3.2 – Applications

This system is a universal scaffold for molecular assembly processes. It moves a solid-phase support to bring reactive moieties on the support in proximity to reactive species that are located at the stable tethered positions along the backbone (sites a-e in figure 1.8). For example, the support could be a controlled-pore glass sphere with a growing DNA strand and the four nucleic acids could be located at the reactive sites; the nucleic acid of choice could be added to the growing chain by moving the bead to the desired position and then introducing polymerase into the system (figure 1.9). The molecular assembly line can also be used for building nanoelectronic devices. The simplest (1-2-3) unit shown in parenthesis in figure 1.8 is a bi-stable toggle switch.
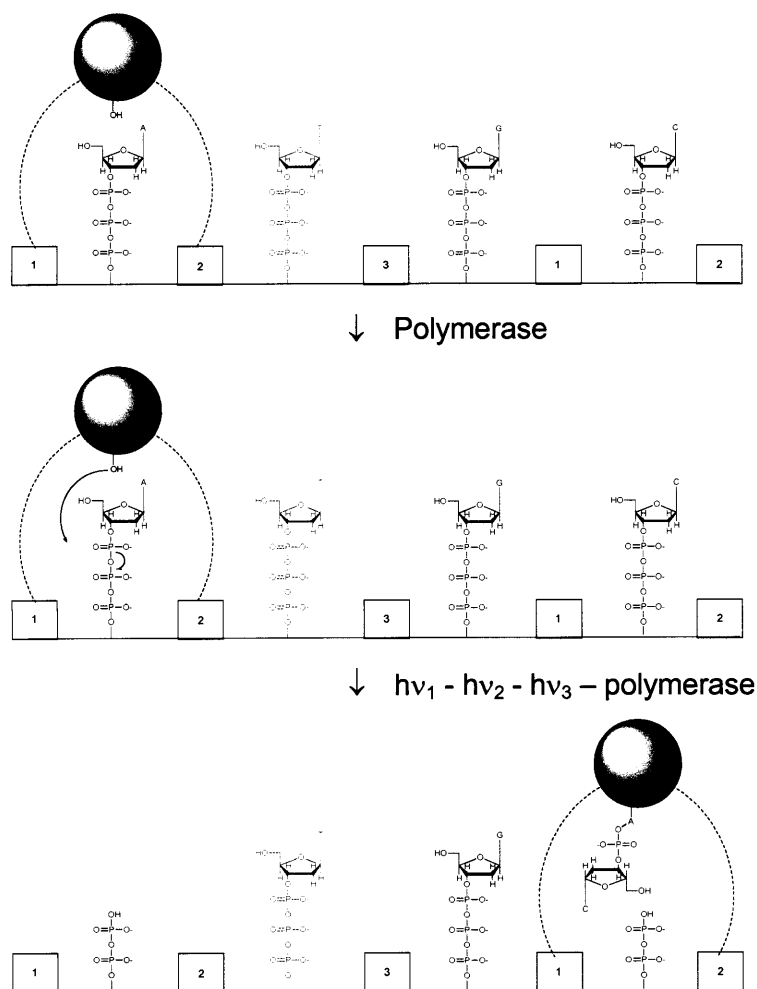
Figure 1.9 Idealized DNA assembly scheme using the proposed molecular assembly line. *Top*: Support is positioned over an adenine residue. *Middle:* Polymerase is added and the nucleotide is now on the solid-support while a diphosphate is left on the polymer backbone. *Bottom:* The support is positioned over a cytosine residue and the enzymatic coupling step occurs again.

Weck *et al.* have also proposed a "universal polymer backbone" (figure 1.10) that is also based on biological molecules [Weck03]. In the Weck scaffold, monomers are polymerized into co-polymers with desired periodicity by ring-opening methathesis (ROMP) reactions. Following the construction of this peptide-like backbone, an "orthogonal self-assembly" step functionalizes the scaffold into novel materials. This backbone is driven by self-assembly and designed for combinatorial materials synthesis. The molecular assembly line differs from the universal backbone proposed by Weck in that the assembly line is designed for dynamic and programmable assembly post-scaffold-synthesis.
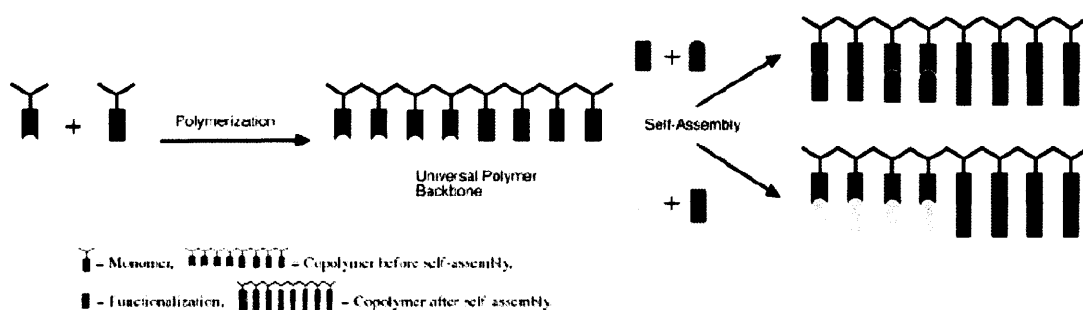
Figure 1.10 "Universal polymer backbone" currently being developed by Weck *et al.* Monomeric units are polymerized into co-polymers by ring-opening metathesis reactions. After the universal backbone is constructed, it is functionalized by orthogonal self-assembly mediated by hydrogen bonds. Image from [Weck03]

1.3.3 – Potential shuttle/antennae interactions and backbones

There are a wide range of potential shuttle/antennae interactions that can be used to build a molecular assembly line, some of which are listed in figure 1.11. Essentially, any set of antennae with three resolvable inputs can create a molecular assembly line. As can be seen in the table, input resolvability and destructiveness, and backbone synthesis are the major issues in choosing the interaction type.

In this thesis, experimental data will be presented on the shuttle/antennae interactions in the first two proposed systems, remote electronic control of DNA hybridization state (Chapter 2), and competitive Michael addition and Norrish Type II photocleavage reactions (Chapter 4). A fully polymerized molecular assembly line has not been constructed, but routes towards them for each approach will be discussed in the respective chapters.

Interaction	Input	Pros	Cons
Figure 1.11 Conceivable shuttle/antennae interactions in the molecular assembly line			
Remote electronic DNA hybridization [Hamad02]	RF coupled into covalently attached nanocrystal antenna	- Highly scaleable backbone. - Non-destructive input. - Potential applications in biophysics	- Resolvability of input frequencies
Reversible covalent chemistry	Simultaneous Michael additions and wavelength selective Norrish Type II photocleavage reactions	- Resolvable by wavelength - Covalent hand-off mimics polyketide synthase - Potential applications in protecting group chemistry	- Destructive input ($210 < \lambda < 310nm$) - Polymer backbone not easily synthesized - Highly basic environment is bad for assembly
Conformational switching and isomerization [Petty95]	Blocking interactions b/w phenylalanine and cyclodextrin host by UV-induced conformational changes in azo compounds.	- Cyclodextrin chains have been synthesized in the literature.	- No wavelength selective azo-compounds have been reported.
Electrostatic [Petty95]	Light driven charge transfer complexes (TCNQs).	- Various complexes known to absorb UV-visible light with reasonably resolvability and over the entire UV-visible spectrum.	- Charge creates highly acidic or basic local environments that are bad for assembly - Polymer backbone not easily synthesized
Metal complex formation [Stoddart01]	Oxidation-reduction state of the complex forces directional movement of a metal-binding ring, such as rotaxanes and catenanes.	- Chemistry is well developed	- Global input requires that local charge be created with electrodes

Chapter 2: RF Biology

2.0 – Introduction to RF Biology

This chapter proposes the design of a molecular assembly line based on selective dehybridization of DNA by coupling a radio-frequency magnetic field into covalently attached nanoparticle antennae that heat the DNA, an idea that will be termed "RF Biology." Experimental work on the monomer unit, a short DNA strand with a covalently attached superparamagnetic nanoparticle, will also be presented.

2.0.1 – Selective dehybridization of DNA

It has been shown that a DNA molecule with a 1.4nm Au nanoparticle covalently attached to it can be selectively dehybridized in a 1GHz RF field [Hamad02]. The RF energy is coupled into the nanoparticle and locally heats the biomolecule while the global temperature of the solution remains constant. Figure 2.1 shows a UV time-course spectrum (260nm) of a DNA hairpin-loop structure in which the DNA hybridization state follows that of the RF on/off cycle. The hairpin-loop is a 38mer with a seven base-pair complement. The peaks in the spectrum represent DNA in its dehybrized state; dehybridized DNA absorbs more UV light at 260nm because of a change in the dipole of the phosphate backbone, a phenomenon known as hyperchromicity.
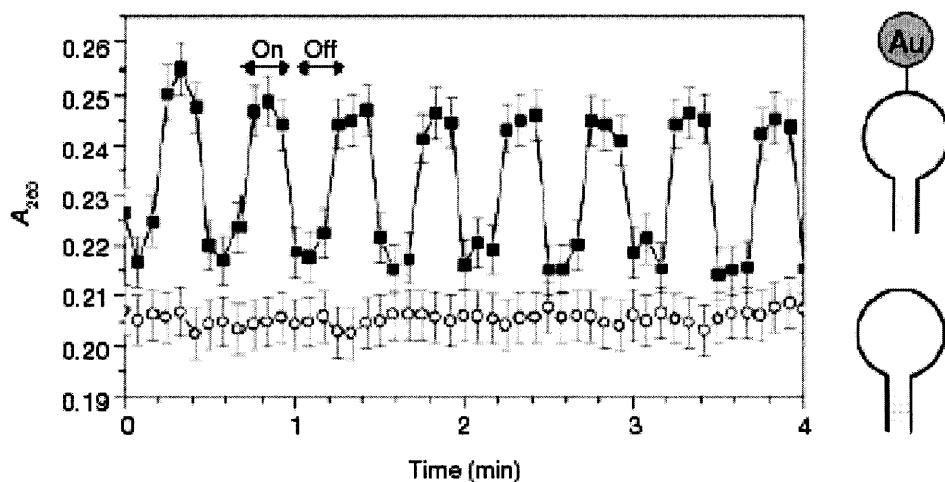
Figure 2.1 Selective dehybridization of a DNA hairpin-loop by coupling 1GHz RF into a covalently attached 1.4nm Au55 antennae [Hamad02].

While the mechanism of local heat generation has yet to be elucidated, it is proposed that the RF inductively heats the metallic nanoparticle. Given this proposed mechanism, there is no resonance frequency at which the DNA is dehybridized, but rather, there is a threshold/basement frequency at 800MHz, above which the localized heating occurs [Hamad, UPR].

2.0.2 – Molecular assembly line based on RF Biology

As will be discussed in section 2.1, the use of superparamagnetic nanoparticles may provide the route to many channels to interface with biology because ferrofluids of superparamagnetic nanoparticles have material and size-dependent resonance absorption frequencies in the RF [Rosenzweig02].

However, let us assume that we have three nanoparticle antennae with resolvable RF absorption bands. Figure 2.2 shows an idealized molecular assembly line based on RF Biology components. Each monomer is composed of a DNA/nanoparticle assembly; the DNA strand is the same for all three monomer units (in the figure, CGTTGC with A_9 spacers). The shuttle in this case could be any non-metallic and non-magnetic solid support that is capped with DNA strands that are partially complementary to the monomer strands (in the figure, GCAACG). Because the control mechanism is localized heating, the nanoparticles must be spaced by a distance d, such that d > R, where R is the radius of a thermal radiation sphere between a point source to T_0. In other words, the heating must be spatially resolved between antennae. Only a (1-2-3) unit is shown for simplicity. M_1 and M_2 represent superparamagnetic nanoparticles with resolvable absorption bands.

There are many advantages in using DNA/nanoparticle assemblies as monomers for a molecular assembly line. The input is non-destructive, as opposed to optical techniques. DNA provides an excellent backbone for the molecular assembly line that can easily be scaled up to yield long assembly lines, and it is even conceivable that engineered plasmids and enzymes could synthesize the molecular assembly lines *in vivo*. Lastly, the ability to locally heat biological molecules and break hydrogen bonds has many potential applications in medicine and biophysics, since hydrogen bond formation is one of the main mechanisms in biological assembly and recognition.

28
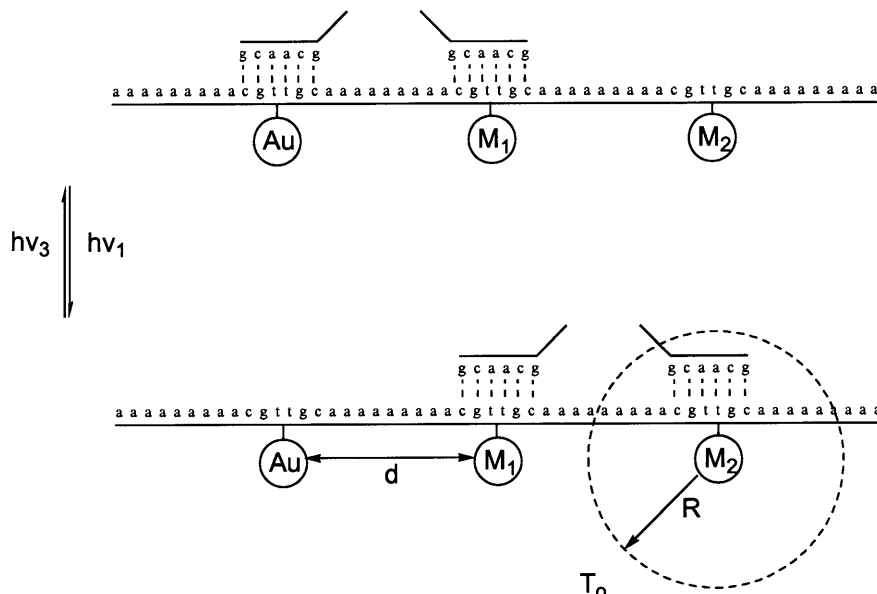
Figure 2.2 Idealized molecular assembly line based on controlling DNA hybridization state by coupling RF into covalently attached nanoparticle antennae.

2.1 – Introduction to superparamagnetic nanoparticles

In electronically addressing a biological molecule using nanoparticle antennae, a reasonable nanoparticle antenna must be fewer than a few nanometers in diameter in order not to dwarf or impede the biological function of the molecules, which are typically 2nm (DNA double helix) to 5nm (typical proteins) in diameter. In this size regime at room temperature, a nanoparticle composed of magnetic elements is considered superparamagnetic.

2.1.1 – Superparamagnetism

Superparamagnets are magnetic particles for which ambient thermal energy is large enough that the magnetization direction cannot be fixed by the anisotropy of the particle [Brown63]. Therefore, at ambient temperature and normal experimental time scales, a superparamagnet has no magnetization in the absence of an external field. At any given temperature, T, the probability P(t) that a particle in some metastable (magnetized) state with energy E_1 will be found in a state having energy $E_2 = E_1 + KV$, is given by the Arrhenius relationship in equation 2.1 – where τ_N is the relaxation time of the magnetic moment, ν_0 and τ_0 are pre-exponential factors (typically, $10^{-9} < \tau_0 < 10^{-11}$ s) and K is the uniaxial anisotropy energy constant that defines a free-energy barrier per unit volume

[O'Handley00]. Equation 2.1 describes a magnetization reversal mechanism of thermal activation over an energy barrier (KV) between two metastable states; the transition probability between these states is a function of the ratio between the barrier KV, and thermal energy k_BT. Figure 2.3 is a picture of the time-dependent magnetization, showing that the magnetization can spontaneously reverse by thermal activation over an energy barrier.

$$P(t) = \nu_o exp(-KV/k_BT) \tag{2.1}$$

$$\tau_N = \tau_o exp(KV/k_BT)$$
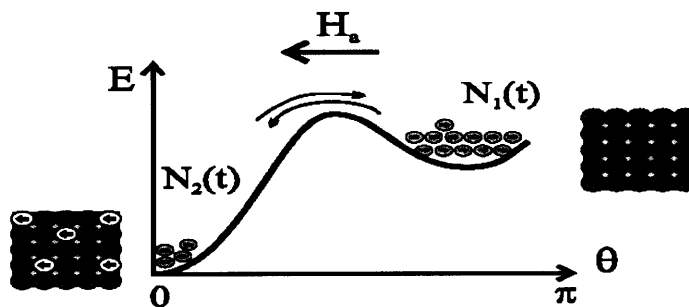
Figure 2.3 Time dependence of magnetization direction θ with respect to an applied field, H_a. N(t) represents the number of particles in a particular energy state with respect to time. The magnetizations can spontaneously reverse by thermal activation over an energy barrier. Image from http://www.essrl.wustl.edu.

Below the "blocking temperature" at which the thermal energy of the system is insufficient to demagnetize the nanoparticle by spontaneous reversal of magnetization, thermal fluctuation is effectively "blocked" and the magnetization remains in a metastable state. Above the blocking temperature and at normal experimental times, a superparamagnet shows no hysteresis in its M-H curve.

Superparamagnets interact with magnetic fields differently at various frequencies. In a static (DC) field, if the particle is free to rotate, it acts as a magnetic dipole and the nanoparticle aligns with the field because it can reduce its energy by aligning its magnetization with the easy (anisotropy) axis and the applied field. In a sufficiently concentrated solution (ferrofluid) or viscous medium, the nanoparticles will form chains because of dipole attractions between particles. In AC fields, the heating mechanisms are due to Brownian losses (kHz), Neél losses (MHz), or ferromagnetic resonance (GHz). These losses are described below. Although, for reasons that will be discussed

in this section, heating by Neél losses was the heating mechanism of choice, it is important to understand each mechanism for future work in designing systems that interface biological molecules with nanoparticle antennae.

2.1.2 – Low-frequency RF losses: Brownian relaxation

At $v \ll 1/\tau_N$, Brownian rotation of the entire particle is the predominant loss mechanism. The entire particle acts as a dipole that tracks the field with the relaxation time, τ_B. The torque (T) on the particle and the power dissipation (P) by viscous drag models [Thompson98] are given in equations 2.3 and 2.4:

$$\tau_B = 3V\eta/k_BT \tag{2.2}$$

$$T = \mu_o \pi R^3 H_o^2 \tag{2.3}$$

$$P = 2N_{particles} \mu_o \pi^2 R^3 H_o^2 \upsilon \tag{2.4}$$

where, η = solvent viscosity, R = particle radius, H_o = applied field strength, and υ = frequency of the AC field.

Power dissipation by viscous drag is the primary cause of heating in magnetic fluid hyperthermia (MFH), a method of destroying tumor cells in low-frequency RF fields by loading them with superparamagnetic nanoparticles. However, the cellular environment is extremely viscous compared to water, in which a molecular assembly line using a DNA backbone would have to be. Furthermore, as can be seen in equation 2.4, it is the size of nanoparticle that primarily affects the power dissipation, and therefore it would be difficult to create localized heating in one antenna (by torque) without influencing all other magnetic nanoparticles in this frequency regime.

2.1.3 – High-frequency RF losses: Neél relaxation

At frequencies on the order of $1/\tau_N$, Brownian motion is essentially frozen out as a mechanism for aligning the particle magnetization with the field. Therefore, the magnetization rotates within the particle to track the field. Losses by this mechanism are known as Neél losses. In a ferrofluid, the magnetization relaxation time τ_{eff} depends on

τ_B and τ_N, but as can be seen in equation 2.5 and figure 2.4a, τ is essentially determined by τ_N for small particles.

$$1/\tau_{eff} = 1/\tau_B + 1/\tau_N \qquad (2.5)$$

$$\chi(\omega) = \chi'(\omega) - i\chi''(\omega) \qquad (2.6)$$

$$\chi(\omega) = \chi_o/(1+\omega^2\tau_N^2) - i\omega\tau_{eff}\chi_o(1+\omega^2\tau_N^2)$$

where χ_o = initial susceptibility

$$P = \pi\mu\chi_o H_o^2\upsilon \, (2\pi\upsilon\tau) / [1 + (2\pi\upsilon\tau)^2] \qquad (2.7)$$

$$\Delta T = P\Delta t/c \qquad (2.8)$$

where c = specific heat

Heat can be generated by Neél losses by the phonons created in the magnetization rotation process. As $\omega\tau$ approaches unity, where ω is the angular frequency, $2\pi\upsilon$, the imaginary suceptibility (χ'') reaches a local maximum and the real susceptibility (χ') passes through a local inflection point (equation 2.6, figure 2.4b) [Fannin02]. The power dissipation also approaches a maximum as $\omega\tau$ approaches unity; the equations for power dissipation and temperature change are given by equations 2.7 and 2.8.
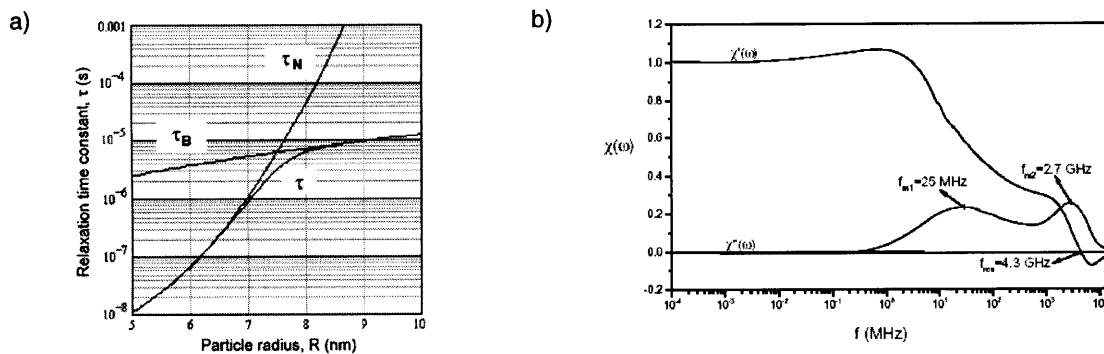
Figure 2.4 a) Ferrofluid relaxation time τ_{eff} as a function of τ_B, τ_N, and diameter. Image from [Rosensweig02]. **b)** Complex susceptibility curves of 8.4nm cobalt nanoparticles. The peak at 25MHz corresponds to maximum power dissipation from Neél losses. Higher frequency resonances are result from ferromagnetic resonance. Image from [Fannin02].

2.1.4 – Microwave losses: Ferromagnetic resonance

At microwave frequencies (GHz), the magnetization cannot track the field by Neél losses. Instead, the magnetization and physical orientation of the particle are pinned along the anisotropy axis by the longitudinal component of the AC field. As the drive frequency approaches the precession frequency of the magnetic moment about the anisotropy axis, ω_o [Fannin99], the magnetic moment can be tipped by the perpendicular component of the field, a phenomena known as ferromagnetic resonance. In FMR, the angular resonant frequency is:

$$\omega_o = \gamma(H_A + H) \qquad (2.9)$$
$$H_A = 2K/M_s$$

where, γ = gyromagnetic ratio, H_A = internal/zero field of a particle, H = applied static field, K = uniaxial anisotropy constant, and M_s = saturation magnetization.

An analogy can be made between FMR and nuclear magnetic resonance (NMR), in the sense that in FMR, the crystalline anisotropy axis acts as an internal static field (H_A) about which the magnetic moment precesses, as opposed to the external static field in NMR. This can be clearly seen in equation 2.9; there exists a natural precession frequency in the absence of an external static magnetic field, and the frequency increases linearly with applied static field, H. FMR in the absence of an applied static field is known as "zero-field resonance."

2.1.5 – Discussion on heating mechanisms

In determining the heating mechanism of choice, several factors must be considered, and each mechanism of heating has its own pros and cons.

First, how do AC fields affect biological molecules in the absence of a nanoparticle? High-frequency fields may cause tissue damage or induce "anomalous backbone vibrations" in DNA [Nuss97]. Second, how do AC fields affect water in the absence of a nanoparticle? The issue of heating water with microwaves is troublesome in the context of the molecular assembly line and more general biomedical and biophysical contexts because it globally affects every molecule in solution. Third, how tight are the resonance

absorption bands of various nanoparticles in the associated frequency range? Developing a set of nanoparticle antennae is necessary for building a molecular assembly line based on RF Biology. It is also desirable for biophysical studies because it would allow one to control many biological molecules independently of one another. Lastly, is the physical process by which heat is generated conducive towards building a molecular assembly line?

Low-frequency Brownian losses are attractive because the AC field will not damage biomolecules or microwave water. However, the ability to find resolvable operating frequencies is an issue. The fact that the entire particle rotates is not desirable for building a molecular assembly line because the rotation of a nanoparticle antenna would affect the entire system.

Utilizing Neél losses is an attractive option because the effects of the AC field on biological molecules and water are limited in the MHz frequency regime. The nanoparticle RF absorption bands are reasonably resolvable. The heat generation is fairly independent of nanoparticle orientation.

Heating by ferromagnetic resonance is an interesting option, primarily because FMR bands are very sharp. However, one runs the great risk of damaging biological molecules and microwaving water at such frequencies.

Given the task at hand, the experimental work in this thesis was directed towards coupling RF in the MHz frequency range, or heating superparamagnetic nanoparticles by Neél losses.

2.2 – Experimental

All reagents were of the highest purity available and were used as received from Sigma-Aldrich unless otherwise indicated. Reactions under nitrogen were performed in a MBraun UniLab glove box unless otherwise noted.

High-resolution TEM micrographs were attained using a JEOL 2010 TEM on copper/Formvar grids from Ladd Research Incorporated. FTIR data was taken using a Digi-Lab Excalibur FTS 3000 (KBr, 64 scans, $4cm^{-1}$ resolution). Fluorescence spectra were obtained using a Jovin-Ybon Spex Fluoromax-3 spectrophotometer (3mm x 3mm quartz cuvette, 1nm slits, 0.5s integration).

2.2.1 – Cobalt nanoparticle synthesis

Synthesis of cobalt nanoparticles was performed under nitrogen. Cobalt chloride ($CoCl_2$, 1.0mmol) and 11-aminoundecanoic acid (2.0mmol) were added in octyl ether (20mL, $0.05M_{Co}$) and heated to 100°C. Tri(octyl)phosphine (3.0mmol) was added, and the solution was heated to 160°C. 1.0M Super-Hydride in THF (2.0mL, 2.0mmol) was added and the solution was stirred vigorously for 20 minutes; the solution color immediately changes from "cobalt blue" to black. Additional Super-Hydride was added (1.0mL, 1.0mmol), and the solution was stirred for 20 more minutes. The reaction was then slowly cooled to room temperature and then removed from the nitrogen atmosphere. The nanoparticles were purified by centrifugation in pure ethanol (approximately 3mg/mL) for 2 hours at 6000g followed by decantation, two times, and then air-dried.

2.2.2. – DNA/nanoparticle assemblies (2)

The DNA hairpin-loop (1) ("stem-loop" or "molecular beacon") was synthesized by Genset Oligos. The terminal nucleotides made up a 7-base-pair stem, with a 24-base-pair loop. The fluorescein dye, FAM, was appended at the 5' end, and the quencher, Dabcyl, at the 3' end. The eighteenth base, denoted as T', was a thymine with an internally modified free amine. The sequence of the oligonucleotide is (5' → 3') given below with the portion in parenthesis representing the "loop" of the hairpin-loop structure:

FAM – GCGCCCT – (AAACTGGTGGT'GGAATGCGTCATG) – AGGGCGC – Dab

Oligonucleotide dehybridization causes an increase in fluorescence, as the efficiency of Dabcyl quenching of FAM fluorescence is distant dependent. The idealized structure of the hairpin-loop and the scenario of increased fluorescence upon dehybridization are shown below in figure 2.5a.

a)

b)
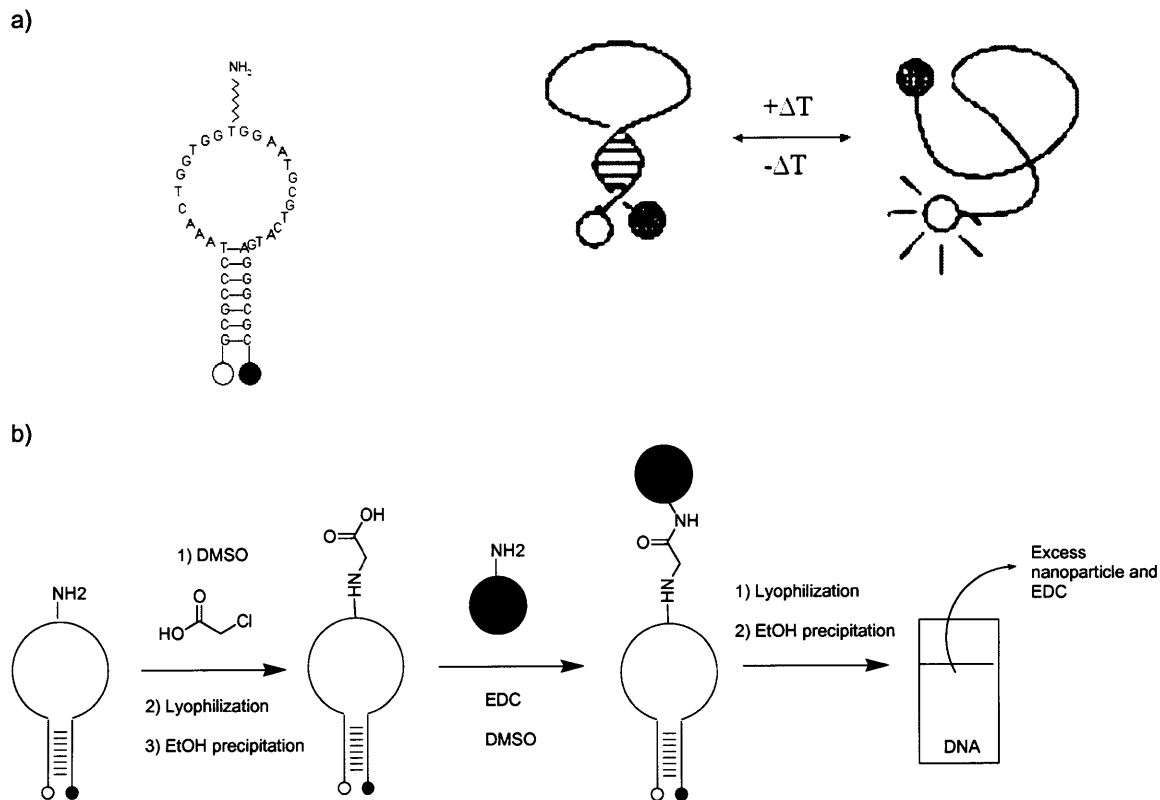
Figure 2.5 a) Idealized structure *(left)* and increased fluorescence upon melting *(right)* of the DNA hairpin-loop. Image modified from [Bonnet99]. **b)** Coupling and purification strategy of covalent attachment of cobalt to DNA hairpin-loop.

Upon receiving the oligonucleotides, a 30μm stock solution was made in DMSO. To obtain carboxylic acid functionalized hairpin-loops, 100μL of the stock solution (3nmol) was shaken overnight with 100μL chloroacetic acid in DMSO (300μM) (10x, 30nmol) at room temperature, using standard nitrogen techniques. The oligonucleotide was purified by overnight ethanol precipitation and then redispersed in 500μL DMSO. A tenfold excess of cobalt nanoparticle (3mg, approximately 30nmol) and a large excess of ethyldiethylaminopropylcarbodiimide (EDC) were added and the solution was shaken overnight. The sample was lyophilized, and then purified by overnight ethanol

precipitation. The DNA/nanoparticle assembly (2) was recast in 1x PBS buffer to make a 1μM solution. The coupling scheme is shown in figure 2.5b.

2.2.3 – Application of RF to DNA/nanoparticles

Typical fluorescence spectra were averaged four times with, λ_{exc} = 495nm.

In order to apply RFMF in the fluoremeter with good global temperature control, a customized cell holder (figure 2.6) had to be constructed to replace the standard cell holder in the spectrophotometer. The cell holder was designed using Rhinoceros 3D modeling software and printed with ABS plastic using a Stratsys 3-D printer. The solenoid (Cu wire, 7 turns, d = 3cm, h = 3cm) was potted using epoxy and painted black to eliminate fluorescence from the polymer. A 0.5cm gap was placed between the solenoid and the cuvette. Water-cooling was provided between the solenoid and sample on the two sides that were not in the light path of fluoremeter to limit radiative heat transfer from the solenoid; the cooled water (15°C) was pumped through Master-Flex tygon tubing with a peristaltic pump, and the top portion of the cuvette that was not in the solenoid core was wrapped with tubing. The entire apparatus was cooled with a small cooling fan (Nidec Gamma 28).

a) b)
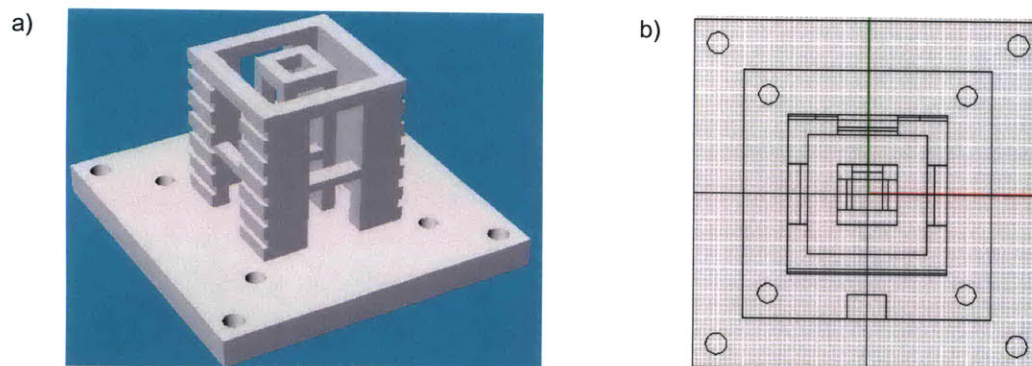
Figure 2.6 a) Perspective view of the spectrometer compatible RF apparatus. **b)** Top-down view as designed in Rhinoceros 3D modeling program.

RF was applied with a HP8648C signal generator coupled with a linear amplifier (+35dBm, 1mW input saturation, 4W output saturation). Because the coil was not impedance matched to 50Ω over all frequencies, the signal generator was driven at maximum output (+14.5dBm) in order to ensure a 4W signal from the amplifier. Prior to RF biology experiments, the power from the generator was increased from 0.0-14.0dBm,

and power after the amplifier was monitored by use of a bi-directional coupler (e-meca) and spectrum analyzer (Agilent E4407B); if the power output from the amplifier saturated before 14.5dBm, a 4W output was assumed. The calculated field strength was 8.2mT.

2.2.4 – Enhanced microwave heating of non-polar solvents

2mL of commercially available ferrofluid of 10nm Fe_3O_4 nanoparticles in a hydrocarbon carrier (FerroTec USA) was dissolved in 8mL hexanes, yielding a 1% volume fraction ferrofluid. The solution was microwaved for two minutes in a commercially available microwave oven (Sharp R214-FW) with a center frequency of 2.45GHz.

2.3 – Results and Discussion

2.3.1 – Cobalt nanoparticle synthesis

The ε-cobalt nanoparticle (NP) synthesis was based on methods reported by Murray [Murray99]. ε-Co or epsilon-phase cobalt is a soft magnetic material whose structure resembles that of the β-phase of manganese. It has a reduced anisotropy from that of HCP cobalt, but can be converted into HCP cobalt by annealing at high temperatures. The low magnetic dipole interactions between particles in this phase during synthesis allows for slower and more controlled nanoparticle growth rates of small superparamagnetic nanoparticles [Murray99][Alivisatos01].

The phosphine provides steric hindrance to slow nanoparticle growth during Super-Hydride reduction. Phosphines weakly bind to the cobalt ions, but are incapable of reducing oleic acid-chelated cobalt ions to form nanoparticles. In general, longer alkyl chains on the phosphine lead to smaller nanoparticles. Murray reports the use of tri(butyl)phosphine yields 7-11nm nanoparticles, and tri(octyl)phosphine yields 2-6nm nanoparticles.

An excess of ligand was used, and the reaction was run at a lower temperature to obtain small nanoparticles. Figure 2.7 shows TEM micrographs and the size distribution of the nanoparticles as synthesized; nanoparticles of 1-5nm were synthesized, with a mean particle size of 2.8nm ($\sigma = 0.7$nm). Because of the induced dipole forces between superparamagnetic nanoparticles during synthesis, it is extremely difficult to achieve one uniform size, especially since the induced dipoles are likely very large when stirring the solution with a magnetic stir bar. Despite reasonably good coarse size control during synthesis, size-selective centrifugation or flocculation is required for fine size selectivity and should be employed in the future. Future work should also employ a mechanical stirrer to lessen induced dipolar attractions during the ripening/growth process, thereby yielding a tighter size distribution in the initial synthesis step.

For the nanoparticles to be covalently bound to biological molecules, terminal reactive functional groups are required, and the nanoparticle must be soluble in aqueous and polar organic solvents. Synthesis with dioic acids ($HOOC-(C_n)-COOH$) led to very large,

gray precipitates, presumably because of bridging between particles, even in the presence of an excess of dioic acid. The aggregates were insoluble in all solvents, even with 15 minutes sonication. TEM showed particle sizes of 100-500nm.

a)

b)

c)
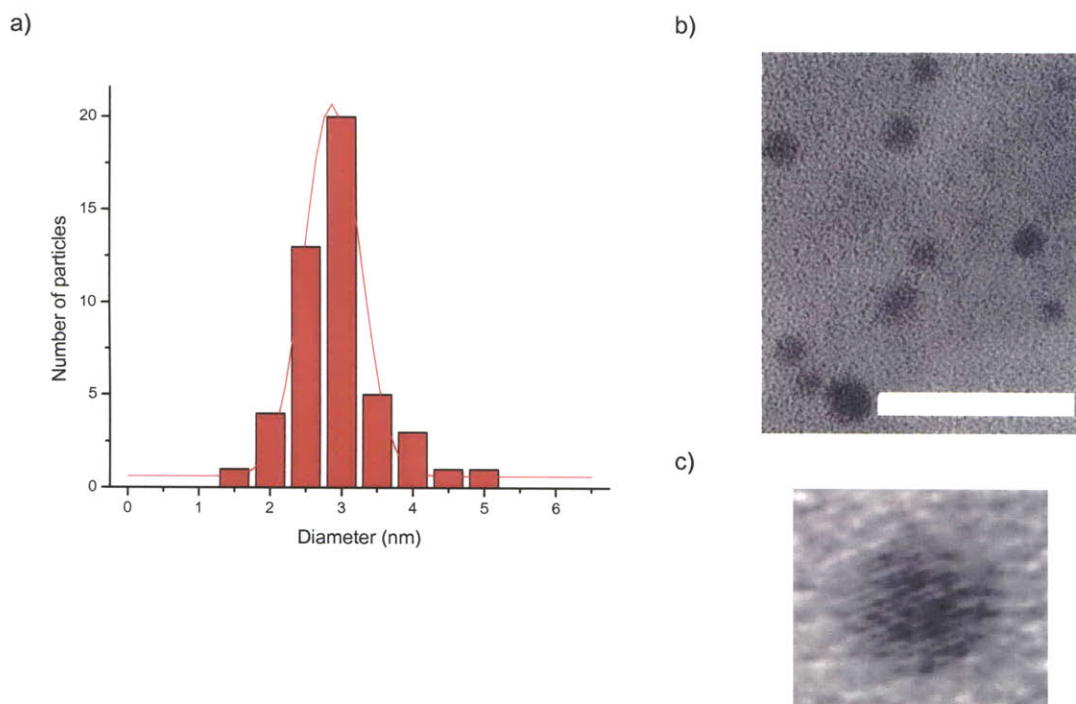
Figure 2.7 a) Size distribution of cobalt nanoparticles obtained from TEM micrographs, with d = 2.8 +/- 0.7nm. **b)** TEM micrograph of cobalt nanoparticles. Scale bar = 10nm. **c)** TEM micrograph of 4nm single crystalline cobalt nanoparticle.

Therefore, 11-aminoundecanoic acid was the preferred ligand, and the coupling reaction of choice between the biomolecule and nanoparticle was for the biological molecule to have carboxylic acids and nanoparticles to have terminal amines. Direct synthesis with 11-aminoundecanoic acid was preferred over the more common strategy of synthesis with long alkyl chain carboxylic acids, like oleic acid, followed by ligand exchange, in order to limit the number of purification steps required and to ensure the percent composition of the terminal group since ligand exchange is a stochastic process.

The nanoparticles were soluble in almost all polar solvents, except for acetonitrile. However, they easily formed aggregates because of the magnetic dipole and hydrogen-bonding interactions between them. The solubility was greatly increased by the addition of a strong acid like1M HCl.

a)
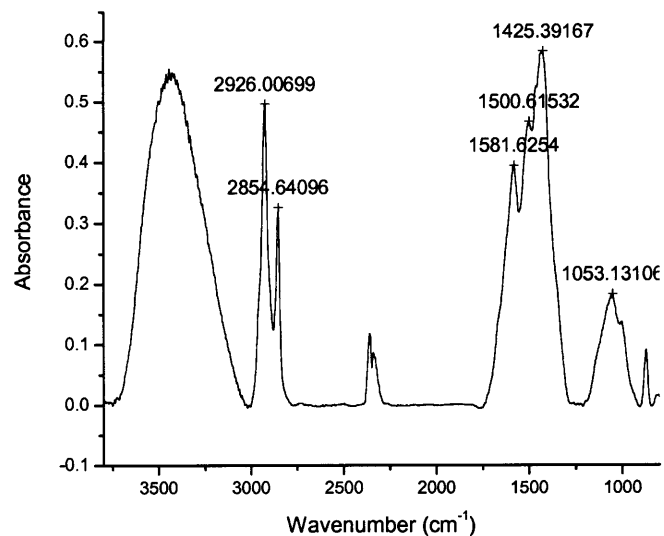
b)
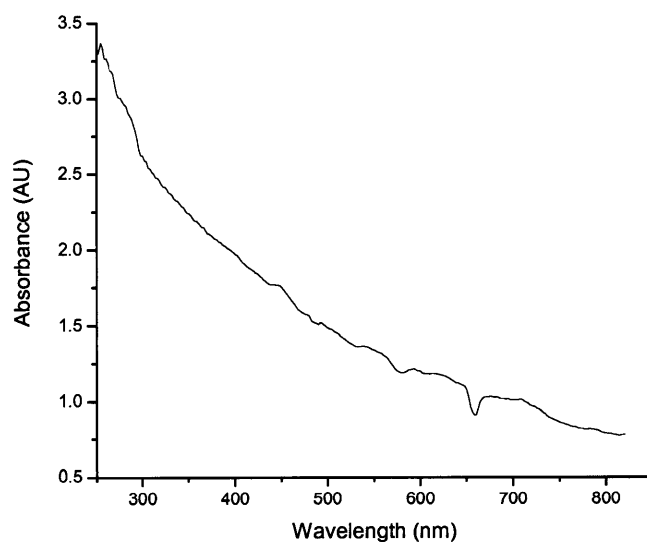
Figure 2.8 Spectroscopic analysis of cobalt nanoparticles. **a)** FTIR spectrum of cobalt nanoparticles. **b)** UV-visible spectrum. The dip around 650nm is an artifact of the spectrometer lamp.

Figure 2.8a show the FTIR spectra of the nanoparticles as synthesized. The nanoparticles show a very broad carbonyl region with peaks at 1581 cm^{-1} and 1425cm^{-1} (carboxylate stretch), and 1500cm^{-1} (C-H bend). The primary amine absorption is most likely buried in the region. Importantly, there is no peak above 1581cm^{-1}, meaning that all the ligands are bound to the nanoparticle by carboxylate bonds and the nanoparticle is amine-capped. Also, the absence of the carboxylic acid peak is fairly good evidence

for the removal of excess ligands. The UV-Visible spectrum in figure 2.8b shows no surface plasmon peaks, which is characteristic of very small nanoparticles. The dip in the spectrum around 650nm is an artifact of the spectrometer lamp.

Despite there being two functional groups on the ligand that are capable of binding to cobalt ions, acids and amines, only the amines are terminal. The ligand is a zwitterion, meaning that at neutral pH, the amine deprotonates the acid, leaving a positively charged ammonium and negatively charged carboxylate; since the metal is cationic, the anionic carboxylate, not the ammonium, binds to the cobalt core. This has been shown in the literature during cobalt nanoparticle synthesis in the presence of oleyl amine and oleic acid [Dumestre02]. It is important that the phosphine and Super-Hydride are added after the ligand is already bound to the metal. If the reducing agents were added with the ligand, the ligand would not be zwitterionic, and this might perhaps make it possible for the amines to bind to the cobalt, leaving mixed terminal functionalities.

2.3.2 – DNA/nanoparticle assemblies

Acrylamide gel electrophoresis of the DNA/nanoparticle assemblies and unlabelled DNA hairpins would indicate that the labeling efficiency was nearly quantitative (figure 2.9). No DNA/nanoparticles can be seen after staining; since the DNA/nanoparticle is net positively charged, it does not migrate towards the positive electrode of the gel, but rather it migrates out of the gel towards the negative electrode. Monofunctionalization (1 nanoparticle : 1 hairpin linkage) was only assumed given the large excess of nanoparticles during the coupling step. Current methods of synthesizing monofunctional nanoparticles based on surface chemistry instead of stoichiometry [Sung, UPR] should be employed in future work.

As figure 2.9b shows, the melting curve of the DNA/nanoparticle assembly is different from the unlabelled DNA hairpin-loop. The melting point is lowered by induced mechanical stress or steric hindrance from the nanoparticle. Also, the fluorescence is greatly quenched by coupling with nanoparticle surface plasmons [Dubertret01]. To account for the effects of destabilization and fluorescence quenching by covalently attached nanoparticles, effective temperatures obtained from fluorescence data are calculated from the melting curves of each individual sample. Therefore, the samples are self-consistent. From here on, the calculated temperature based on FAM emission

will be called "effective temperature." Future work should use DNA hairpin-loops with dyes that emit light at much higher wavelengths to limit quenching.

a)
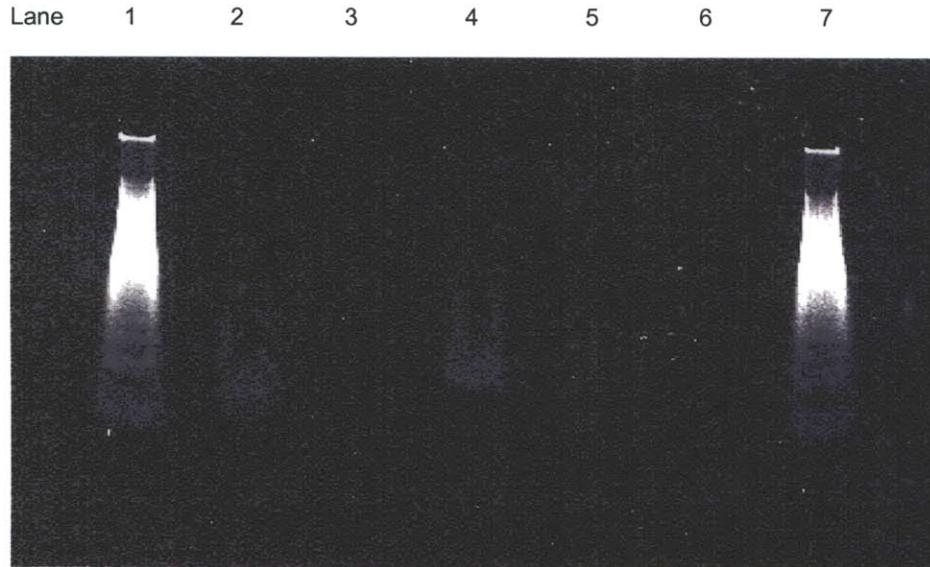
(1,7) = DNA stack, (2) DNA hairpin-loop with no nanoparticle, (3) Cobalt nanoparticle, (4) DNA hairpin-loop + non-covalent cobalt nanoparticle, (5) DNA hairpin-loop with covalently attached cobalt nanoparticle precipitate from ethanol precipitation, and (6) DNA hairpin-loop with covalently attached cobalt nanoparticle supernatant from ethanol precipitation. The net positive charge of DNA with covalently attached nanoparticle causes the assembly to leave the gel. The absence of a spot after staining indicates covalent linkage. The nanoparticle does not pull DNA into the ethanol layer, as evident in lane 6.

b)
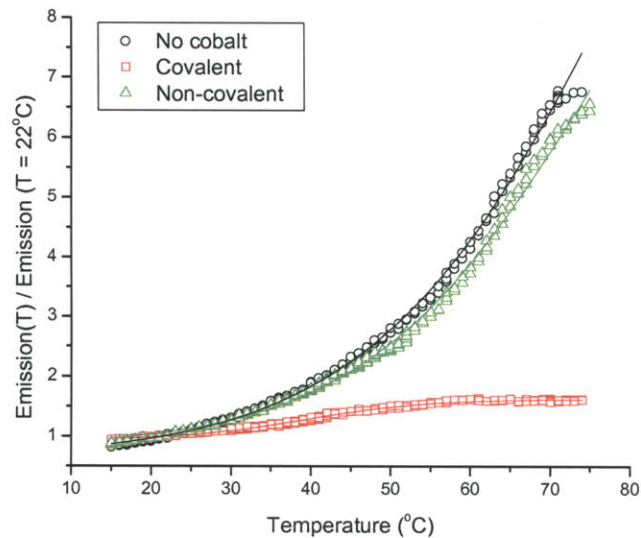
Figure 2.9 a) Gel electrophoresis of DNA/nanoparticle assemblies **(2)**, unlabelled DNA hairpin-loop **(1)**, and a mixture of **(1)** and cobalt nanoparticles. **b)** Melting curves of DNA with no cobalt nanoparticle **(1)** (black circle), non-covalent cobalt nanoparticle (green triangle), and covalently attached cobalt nanoparticle **(2)** (red square).

2.3.3 – Application of RF to DNA/nanoparticles

As can been seen in figure 2.10, the global temperature of 1x PBS buffered water does not change in the RF apparatus with temperature control over one hour continuous irradiation. In figure 2.10a, the frequency was swept from zero to 1 GHz, in 50MHz steps every three minutes. From here on, global heating of the solution from the heat generated by the coil or RF absorption by 1x PBS buffer will be termed "coil heating." Continuous irradiation of 1x PBS buffered water over one hour at 300MHz also showed no evidence of coil heating (figure 2.10b). Global heat created by the solenoid was greatly limited to a temperature variation of +/- 4°C, as measured by a thermocouple (Omega). Even though water-cooling was provided between the cuvette holder and the solenoid, it was extremely important that the top portion of the cuvette was wrapped with tubing and the entire apparatus was air-cooled because the greatest source of coil heating was the heating of quartz cuvette.

a)   b)
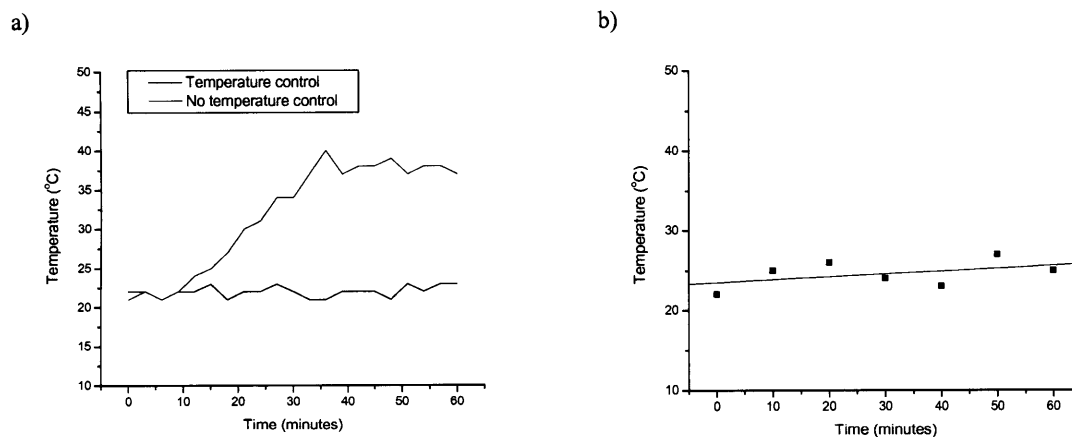
Figure 2.10 a) Global temperature of 1x PBS buffered water under constant RF irradiation over 1 hour. The frequency was increased by 50MHz every 3 minutes from 0-1GHz **b)** Global temperature of 1x PBS buffered water under 300MHz irradiation for one hour.

Figure 2.11 shows the fluorescence spectra of FAM emission (4 scans averaged over 200 seconds) in a 300MHz field. The increased intensity of FAM emission is evidence of selective dehybridization of **(2)** at 300MHz versus **(1)**, which has no nanoparticle antenna that can couple RF. There is a dip in the spectrum of **(2)** around 505nm and a hump around 512nm that are not typically present in the FAM emission spectrum. These aberrations are likely due to surface plasmon (figure 2.9b) coupling between the

metal nanoparticle and dye emission [Dubertret01]. The effective temperature change due to RF is $\Delta T = +18°C$.

a)
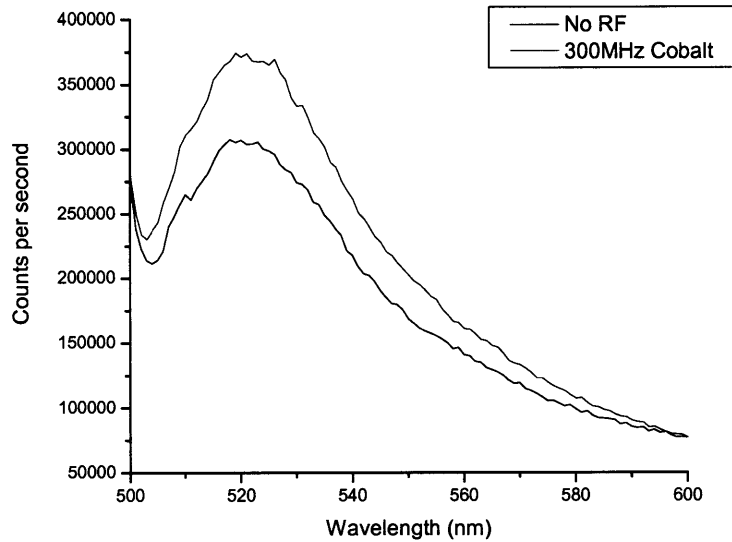
b)
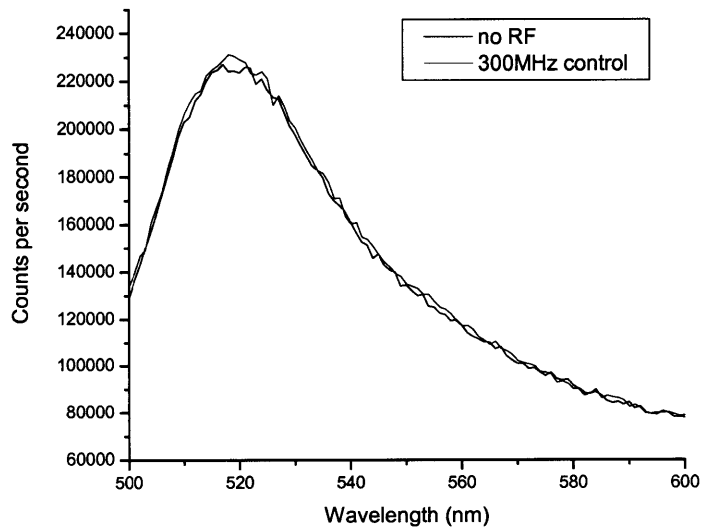
Figure 2.11 Selective hybridization of DNA hairpin-loop with covalently attached 2.8nm cobalt nanoparticle antenna. **a)** Fluorescence spectra of **(2)** in a 300MHz field for 200 seconds (red). **b) (1)** in 300MHz field under the same conditions as in **(a)**.

Figure 2.12a shows the frequency response of the DNA/nanoparticle assemblies **(2)** from 100MHz – 1GHz, measured in 25MHz steps; y-axis data points in figure 2.12a are the fluorescence emission values at 517nm taken from spectra obtained under the same

conditions as in figure 2.11. The frequency dependent selective dehybridization of the DNA hairpin-loop was not related to the field strength at that frequency, as can be seen by the reflected power spectrum of the coil from 100MHz to 1GHz, as measured by an Agilent 8417E RF network analyzer (figure 2.12b). Even though slight RF induced dehybridization occurred at all frequencies measured, the response was fairly resonant, with a Gaussian fit showing a full-width-half-maximum (FWHM) of approximately 40MHz.

a)
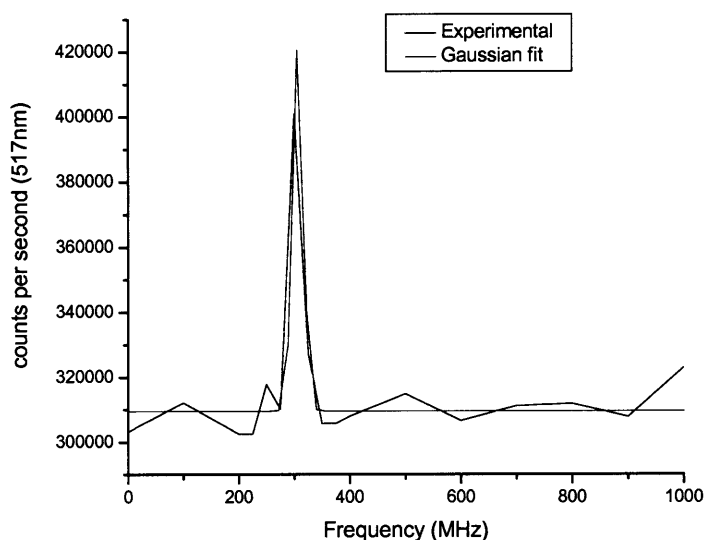
b)
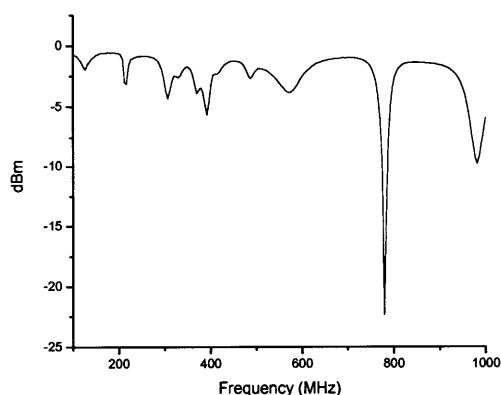
Figure 2.12 a) Maximum FAM emission vs. frequency from (2). The Gaussian fit shows that RF coupling into the nanoparticle antennae is resonant, centered at 306MHz with FWHM = 40MHZ (or σ = 20MHz). b) Reflected power spectrum of the coil; the response of (2) was not related to the field strength of the coil.

While the response was not truly "resonant" like quantized UV electron transitions, a 40MHz FWHM would certainly be sufficient for building a molecular assembly line based

on RF Biology. The result would lead one to believe that another nanoparticle antenna of different composition could selectively dehybridize an oligonucleotide at another resolvable frequency below 800MHz (the cutoff of Au_{55}), meaning that the RF Biology approach is a reasonable one towards constructing a molecular assembly line.

In the more general biomedical and biophysics contexts, it is extremely convenient that (2) responds well below microwave frequencies. 300MHz is a reasonable operating frequency for biophysical studies and biomedical applications considering that current NMR spectrometers / MRI machines usually operate from 200 – 500MHz. It is desirable in biomedical applications that the lowest frequency possible be used in order to limit undesirable tissue damage [Hergt98] and to prevent inducing random backbone vibrations in oligonucleotides and proteins [Nuss97].

This work assumed a steady-state heating model. The effective temperature was calculated from measurements that had to be made by averaging many scans over the time span of minutes primarily because of instrument noise and the acquisition time of the spectrometer. No matter what the application, but especially if one wishes to build a molecular assembly line based on RF Biology, RF would ideally be applied for as short a time as possible and not for minutes as in this study. Future work should include single molecule kinetic studies with known heat transfer constants; to test the hypothesis that the system is one-dimensional transient conduction, the conduction and convection rates must be known for interfaces between DNA/nanoparticle/solution as well as the interface between the solution/cuvette/cooling mechanisms. The spectrometer should be able to acquire data at a frequency greater than the applied RF frequency to observe the time evolution of heat generation and selective dehybridization.

While global temperature changes were monitored with a thermocouple before and after the RF was applied, there were no direct temperature measurements during RF application because electronic thermometers (thermocouple and IR thermometer) could not function properly in the presence of the RF. The physical constraints of the spectrometer made it impossible to use a non-electronic thermometer. Therefore, future work should also employ an internal temperature standard, such as another DNA hairpin-loop with a different fluorophore with no covalently attached nanoparticle antennae.

2.3.4 – Enhanced microwave heating of non-polar solvents

Figure 2.13 shows the global temperature of a 1% volume fraction ferrofluid of 10nm Fe_3O_4 nanoparticles in hexanes and pure hexanes heated in a commercial microwave oven. The global temperature of the ferrofluid increases at a much faster rate than pure hexanes as a result of coupling energy into the nanoparticles by FMR. The global temperature increase in the pure hexanes sample, which is non-polar, is likely a result of microwave heating of the vial. Fannin *et al.* have shown that 10nm Fe_3O_4 nanoparticles in a hydrocarbon carrier (1.8% volume fraction in Isopar M) exhibit a zero-field FMR peak around 2.2GHz [Fannin01]. Even though a commercial microwave oven is designed for a center frequency of 2.45GHz, its spectrum is typically very broad and includes electromagnetic waves at 2.2GHz.
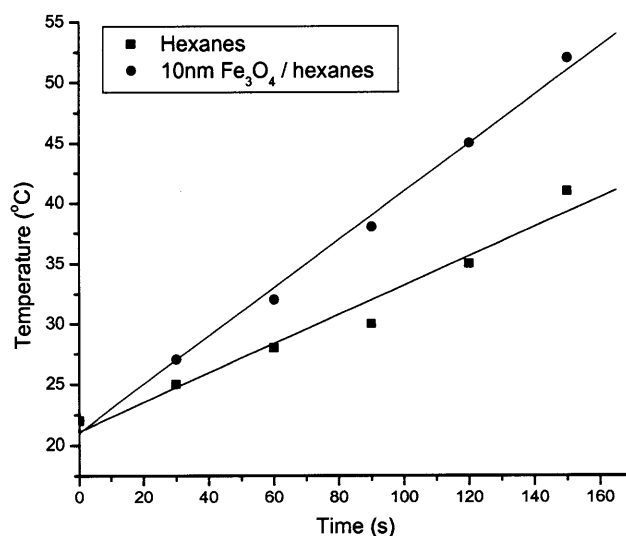
Figure 2.13 Enhanced heating of hexanes solution by ferromagnetic resonance heating of 10nm Fe_3O_4 nanoparticles.

FMR provides an interesting route towards localized heating of biomolecules through nanoparticle antennae because the resonance frequency bands are typically very sharp, and thus may provide many resolvable operating frequencies. However, as mentioned in section 2.1.5, microwave frequencies may cause damage to biological molecules, often by anomalous backbone vibrations [Nuss97]. Since the zero-field FMR frequency is primarily determined by nanoparticle size and composition, the resonant frequency for nanoparticles of desirable size to interface with biology would likely be far greater than

2.2GHz, which is undesirable due to the efficient microwave absorption by water at those frequencies.

Chapter 3: DC Biology

3.0 – Introduction to DC Biology

This chapter discusses the control of secondary protein structures in the presence static magnetic fields. The novel synthesis of magnetic wires that are exactly one molecule wide is also discussed.

3.0.1 – Control of biological molecules using static magnetic fields

In recent years, much work has been conducted on the manipulation of biological molecules and cells in the presence of static magnetic fields using superparamagnetic nanoparticles. Magnetic tweezers capable of applying and measuring piconewton forces are often used for biophysical studies like determining the relaxation mechanism of DNA supercoils by topoisomerase, or biological sensing studies like real-time PCR monitoring [Croquette00] (figure 3.1). The combination of magnetic fields and fluid flow has been used to separate cell/magnetic bead conjugates from unlabelled cells [Bacri00].
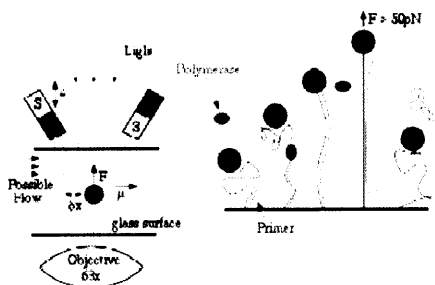
Figure 3.1 Real-time PCR monitoring using static magnetic fields. A single-strand DNA template (plus short complementary PCR primer) is tethered between a glass surface and a magnetic bead that is held fixed with a magnetic field. As polymerase synthesizes the complement, a significant force on the bead results from the DNA chain extension, causing bead movement that is monitored under microscope. Image from [Croqette00].

In the presence of a magnetic field, the induced dipolar attractions (N-S) and repulsions (N-N, S-S) cause supeparamagnets to form chains along their anisotropy axes in a sufficiently viscous environment in which diffusion is limited. Chain formation and crystalline alignment will lead to observable room temperature hysteresis in a M-H curve, as can be seen in figure 3.2, which show M-H curves of the single-molecule magnet (section 3.0.2) Mn12-acetate **(4)**, with and without field-alignment.
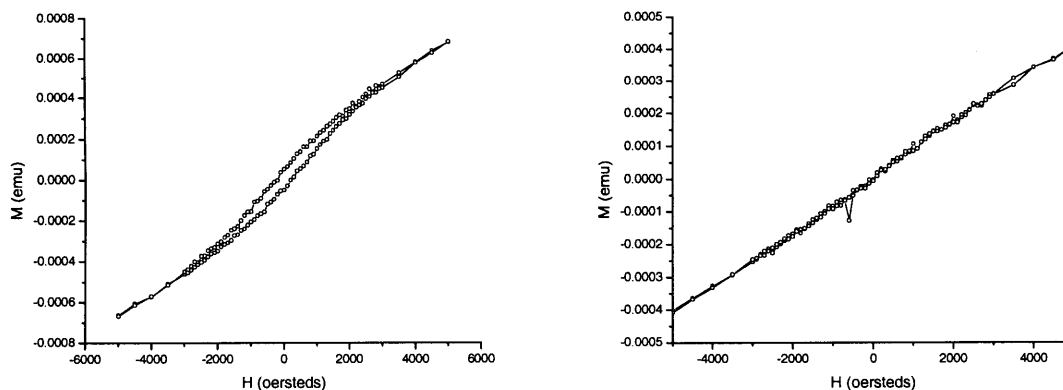
Figure 3.2 M-H curves of Mn12-acetate **(4)** with (left) and without (right) field alignment. Room temperature hysteresis is observed in the field-aligned sample. The field-aligned sample was measured along the axis of alignment.

Simple chain formation of superparamagnets in the presence of a magnetic field can potentially be used to alter secondary protein conformations, as shown in figure 3.3. In the figure, two superparamagnetic nanoparticles that are covalently linked to the ends of an α-helix are separated by the helix by a distance r_1 in the absence of a magnetic field. In the presence of a magnetic field, if the magnetic dipole attraction is large enough, the nanoparticles will exert enough force (torque) to induce an α-helix/random-coil transition in the protein secondary structure, such that the nanoparticles will be separated by a shorter distance r_2. These changes would be observable by circular dichroism (CD) or SQUID magnetometry measurements. The figure also shows how an organic linker molecule of length greater than or equal to r_2 can be used to covalently bridge the nanoparticles once the induced conformational change has occurred, allowing one to lock the protein in its less thermodynamically favored state in the absence of a magnetic field and effectively, "turn off" the protein permanently.

Because the input is DC, there is only one possible input, making this control of protein secondary structures useless towards building molecular assembly lines. However, it was explored nonetheless since the ability to control protein secondary structures would be an extremely useful tool in biophysics.
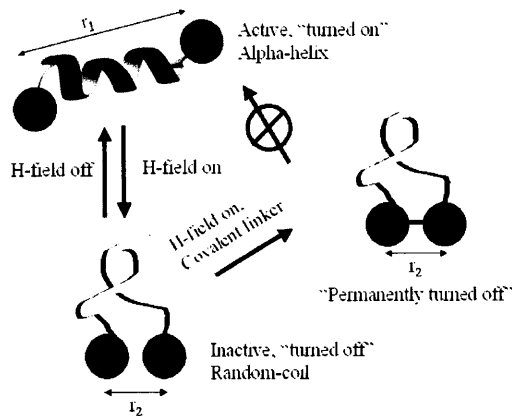
51

3.0.2 – Single-molecule magnets: Special superparamagnets

A special class of superparamagnets are dodecanuclear manganese species with the formula $[Mn_{12}O_{12}(RCO_2)_{16}(H_2O)_4]\bullet(RCO_2)_2(H_2O)_4$, often called single-molecule magnets or SMMs [Lis80] [Sessoli93]. Figure 3.4 shows the structure of a typical SMM. It is comprised of 8 Mn(III) ions that form a crown around 4 Mn(IV) ions that make up an inner cube. The MnO core is less than 1nm in diameter, and the total hydrodynamic radius is less than 2nm.
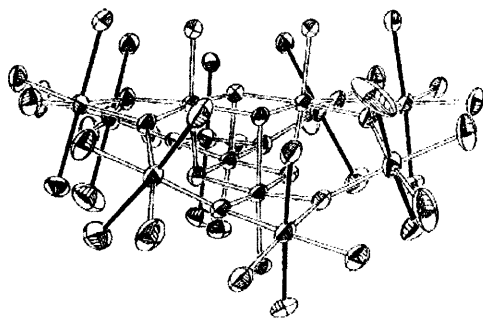
a)   b)
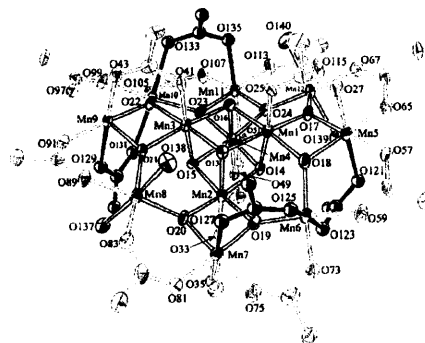
Figure 3.4 a) Typical $Mn_{12}O_{12}$ core of single-molecule magnets with the formula $Mn_{12}O_{12}(RCO_2)_{16}$. The solid black lines represent Mn-O bonds that lie on the Jahn-Teller axis. These ligands can be selectively exchanged due to the decreased bond energy that results from their distorted shape. **b)** Structure of $Mn_{12}O_{12}(RCO_2)_{12}(NO_3)_4$ showing the sites of selective ligand abstraction, represented by the solid black lines. Images from [Christou01].

SMMs have large anisotropy energies, almost that of bulk materials, due to Jahn-Teller distortions in the coordination of the carboxylate ligands about the Mn ions. Their long Neél relaxation times ($\tau_0 \sim 10^{-7}$s) result from geometric spin frustration between the crown Mn(III) and cube Mn(IV) ions.

These species are very attractive nanoparticles to covalently attach to biological molecules. First, they are molecular (as opposed to colloidal) and thus, have an exact and small size. Second, it has been shown that the four carboxylate ligands with both oxygen atoms lying on Jahn-Teller axes can be selectively abstracted [Christou01] (figure 3.4b) because of the decreased metal-ligand bond strength that results from the Jahn-Teller shape distortion; therefore, it is possible to guarantee covalent attachment at a particular site and along a particular crystalline axis.

The initial interest in these species was in their potential use as antennae for selectively dehybridizing DNA with RF, but they could not generate enough heat to do so. However, they may be suitable for controlling peptide conformations, as described in section 3.0.1. Furthermore, they make interesting precursors in the synthesis of molecular magnetic wires that are exactly one-molecule wide, or rather a pearl necklace of covalently linked superparamagnets that are aligned along one axis by purely chemical means.

3.1 – Experimental

All reagents were of the highest purity available and were used as received from Sigma-Aldrich unless otherwise indicated. Reactions under nitrogen were performed using standard techniques. High-resolution TEM micrographs were attained using a JEOL 2010 TEM on 200 mesh copper/Formvar grids from Ladd Research Incorporated. FTIR data was taken using a Digi-Lab Excalibur FTS 3000 (KBr, 64 scans, $4cm^{-1}$ resolution). Room temperature M-H curves were obtained using a Lakeshore Scientific vibrating sample magnetometer (VSM) in epoxy. Circular Dichroism spectra were obtained with an Aviv Instruments Circular Dichroism Spectrophotometer Model 202 (3s collection time, 1nm per 1s steps). EDAX analysis was performed on an FEI DB-235 focused-ion-beam microscope (FIB) equipped with an EDAX Phoenix analyzer.

3.1.1 – Peptide/nanoparticle assemblies

Peptides were synthesized at the MIT Biopolymers Laboratory using standard FMOC/DDE synthetic techniques on chlorotrityl resins, and were received cleaved from the resins. The sequence was $(AAKK)_8A$ (1). Upon receiving the peptides, 0.05g/mL (~0.02mmol/mL) stock solutions were made in DMF. Cobalt nanoparticles were synthesized as described in section 2.2.1. Mn12-tuBu/nitrate was synthesized as described in section 3.1.3.

First, 25μL piperidine was added to 100μL stock solution (2μmol peptide, 20% piperdine v:v) and shaken for 15 minutes at room temperature, and purified by cold ether precipitation (90% v:v, -20°C). The N-terminus was converted to a carboxylic acid by treating the peptide with 100μL of 1M chloroacetic acid in DMF (0.1mmol, 500x), shaking the solution for 30 minutes, and purifying by ether precipitation. The peptide was then recast in DMF.

18mg cobalt nanoparticles (~10x) and 38mg EDC (100x) were added to 1μL peptide (20nmol). 99μL DMF was then added, and the solution was shaken overnight, followed by purification by ether precipitation. DDE side chain protecting groups were removed by treatment with 100μL of 2% (v:v) hydrazine monohydrate in DMF for 30 minutes. After purification by ether precipitation, the resultant cobalt labeled peptide (2) was recast in 1x PBS.

Mn12-tBu/nitrate labeled peptides (3) were prepared as described above, except 5mg (6) (20x) was added with no coupling agent, in place of cobalt nanoparticles and EDC.

3.1.2 – Field-induced changes in secondary protein structures

Circular dichroism measurements were made in the presence of a magnetic field by placing a small permanent magnet under the cuvette; the position of the cuvette in the spectrometer was not altered by the presence of the magnet.

3.1.3 – Synthesis of molecular magnets and magnetic wires

All single-molecule magnet syntheses were verified by comparison of FTIR spectra with reported literature spectra.

Mn12-acetate (4) $[Mn_{12}O_{12}(CH_3CO_2)_{16}(H_2O)_4]$

Synthesis of (4) was based on literature methods [Lis80]. 4.0g (16.3mmol) $[Mn(CH_3CO_2)_2 \bullet 4H_2O]$ was dissolved in 40mL 60% (v/v) acetic acid (aq). 1.0g $KMnO_4$ (6.4mmol) (Mallinckrodt) was added and the solution was stirred for two days at room temperature. The red powder was collected by vacuum filtration and washed with copious amounts of acetone and THF. The disordered acetate ligands in $[Mn_{12}O_{12}(CH_3CO_2)_{16}(H_2O)_4] \bullet (CH_3O_2)_4$ were removed by toluene azeotrope (2 x 75mL) followed by vacuum filtration and washing with acetone, and then the process was repeated.

Mn12-tBu (5) $[Mn_{12}O_{12}(tBu-CH_2CO_2)_{16}(H_2O)_4]$

Synthesis of (5) was based on literature methods [Christou01]. 2.0g (1mmol) of (1) was dissolved in 50mL toluene and treated with 2mL tert-butylacetic acid. Toluene and acetic acid (azeotrope) were removed under vacuum. 50mL of toluene was added and removed by evaporation. After the entire process was repeated, the slurry was dissolved in 50mL toluene and filtered. The collected solid (5) was washed with hexanes and dried under vacuum.

Mn12-tBu/nitrate **(6)** [$Mn_{12}O_{12}(tBu-CH_2CO_2)_{12}(NO_3)_4(H_2O)_4$]

Synthesis of **(6)** was based on literature methods [Christou01]. 0.1g (0.04mmol) of **(5)** was dissolved in 5mL acetonitrile and treated with 900μL of 0.226M HNO_3 (in acetonitrile). The slurry was stirred for one hour. 2.5mL nitromethane was added, and the solution was filtered. The collected solid was washed with ether and dried under vacuum.

Molecular wires based on Mn12-acetate **(7)**

0.05g (0.025mmol) **(4)**, 0.176g (1mmol) hexamethylene diamine, and 235μL diisopropylcarbodiimide (DIC) (1.5mmol) (Avocado) were stirred under N_2 in 35mL CH_2Cl_2/ acetonitrile (1:1 v/v) for three days. SMM chains precipitated from solution. Excess DIC, diamine, and unchained Mn12-acetate were removed by decantation. 35mL acetonitrile was added and the solution was decanted again. The sample **(7)** was dried under vacuum.

3.2 – Results and Discussion

3.2.1 – Peptide/nanoparticle assemblies

Figure 3.5a shows the CD spectra of unlabelled peptide (1) (black squares), cobalt-peptide (2) (red circles), and SMM-peptide (3) (green triangles); figure 3.5b shows the literature reported spectra of poly-L-lysine as a reference for the trends in helix-coil transitions. The typical "camel's hump" between 215-230nm that is characteristic of α-helices are present in all three. The spectrum of (1) appears to be that of a combination of a random-coil and α-helix, probably because of the short length of the peptide and low concentration. The spectrum of (3) has significant contributions from the Mn12-tBu/NO$_3$, especially in the carboxylate region around 280nm.

a)   b)
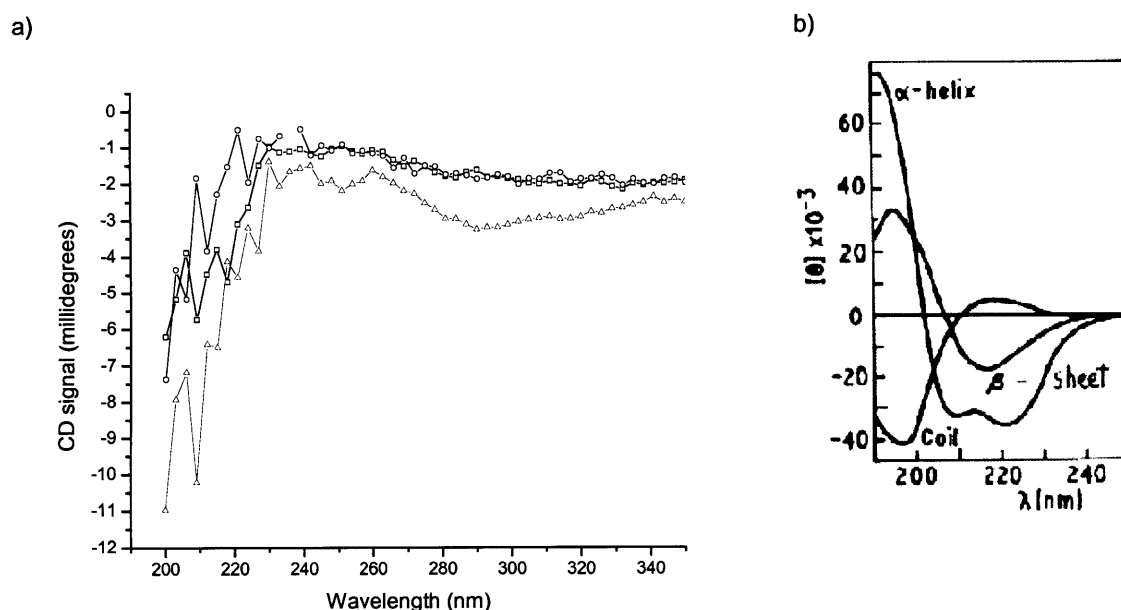
Figure 3.5 a) Circular dichroism spectra of peptide **(1)** (black square), cobalt-peptide **(2)** (red circle), and SMM-peptide **(3)** (green triangle) **b)** Spectra of poly-L-lysine, taken from [Campbell84].

While single-molecule magnets because of their size are the ideal superparamagnets for inducing conformational changes in protein secondary structures, the presence of the magnetic field changes the CD spectra of a single-molecule magnet, indicating a coupling between the induced magnetic dipole (spin) and the absorption of circularly polarized light. Future work should focus greatly on this coupling. However, at this time, not enough data on the field-induced changes in the CD spectra of SMMs is available to

be able to report the effect of the magnetic field on the peptide conformation, since the contributions of the SMM to the spectrum of (3) in the presence of a magnetic field cannot be subtracted out with the available data.

3.2.2 – Field induced changes in secondary protein structures

Figure 3.6a shows the effect of the magnetic field on the spectrum of (2) with (black) and without (red) the magnetic field. The magnetic field appears to induce random coil formation in (2) (black), as evident by the greater (linear) slope in the curve at lower wavelengths, between 210-220nm, at which the contributions of the random-coil to the spectra should dominate. Given the space constraints inside the spectrometer, only a very small permanent magnet was placed under the cuvette, so it is likely that only a small fraction of the nanoparticles were magnetized. The conformational changes should be far more detectable with a different experimental setup in which the entire cuvette is surrounded by magnets. These efforts are currently underway, as well as larger scale preparations of (2) for less noisy spectra, extensive temperature scans to evaluate the effect of cobalt nanoparticles on the stability of the α-helix, and the preparation of assemblies with different peptides that may form more stable α-helices.
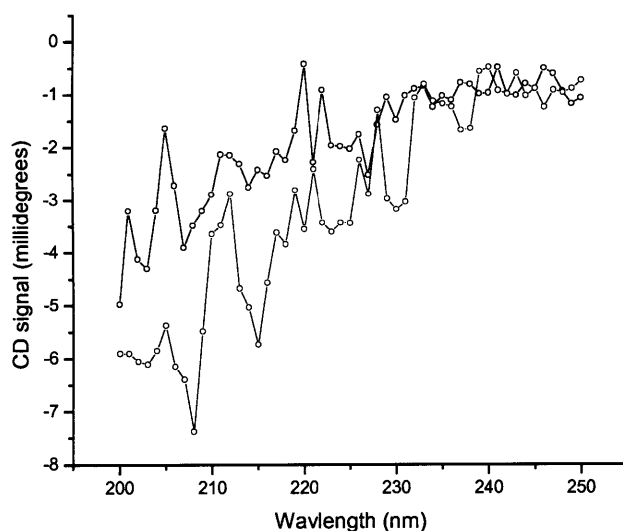
a)   b)
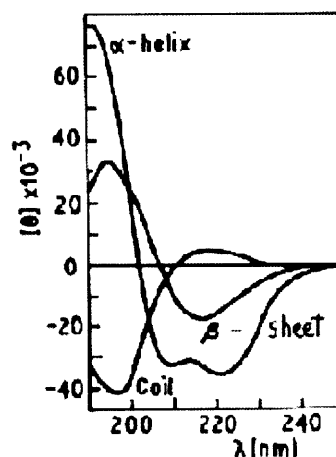
Figure 3.6 Induced α-helix to random-coil transition due to induced dipole interactions between cobalt nanoparticles. **a)** Circular dichroism spectra with (red) and without (black) a small magnetic field. **b)** Spectra of poly-L-lysine. Image from [Campbell84].

3.2.3 – Synthesis of molecular magnets and magnetic wires (7)

While site-specific ligand abstraction in SMMs has been shown in the literature [Christou01], reactions attacking those chemically labile sites have yet to be shown. Figure 3.7 shows the FTIR spectra of Mn12-acetate (4) and the molecular magnetic wires (7). It is believed that the SMM chains (7) were formed via deprotonated amide bonds at the chemically accessible carboxylate sites in which both oxygen and nitrogen are involved in coordinating the ions. It is important to note that these changes in the spectra persist after multiple purification steps, which would indicate that they are not from unreacted hexamethylene diamine.
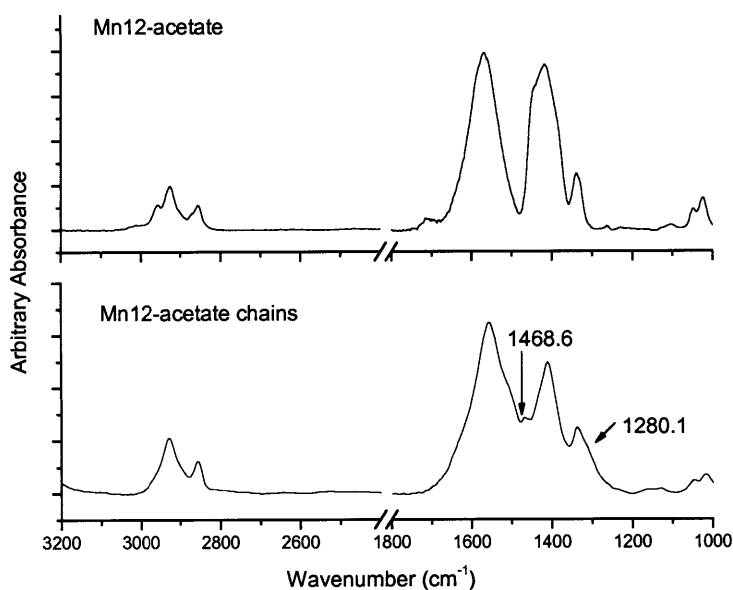
Figure 3.7 FTIR spectra of Mn12-acetate (1) and Mn12-acetate molecular wires (8).

The spectrum for (7) shows an increase in intensity in the alkyl regions (2929 and 2857cm^{-1}) relative to carboxylate peaks (1567 and 1417cm^{-1}) and a new peak at 1468cm^{-1} (CH$_2$ bend) that indicates the presence of the methylene groups from hexamethylene diamine. The significant increase in relative intensity of the peak at 1567cm^{-1} versus 1417cm^{-1} indicates the presence of N-H groups (N-H bends). Changes in the carboxylate region of (7) (broadening, increase in the 1567cm^{-1} peak intensity, and the new peak at 1468cm^{-1}) may also be attributable to the formation of deprotonated amides that replace four (25%) of the carboxylate ligands. The most telling evidence for the formation of deprotonated amides is the broadening in the $v < 1336$cm^{-1} region and

the hump at 1280cm^{-1} in **(7)**, which are unique to metal-chelated nitrogen atoms and are not present in amines [Nakamoto68].

a)
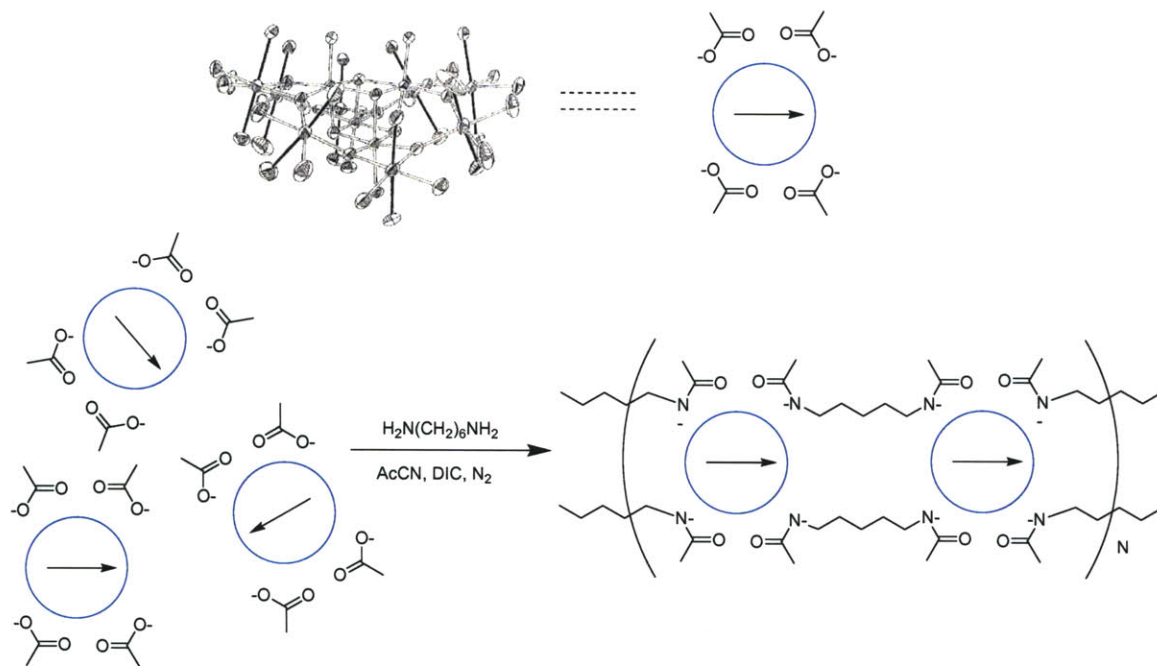
b)

Figure 3.8 a) Proposed route towards molecular wires composed of a string of individual single-molecule magnets with aligned crystalline axes. **b)** TEM micrograph of molecular wires **(7)**. Scale bar = 10nm.

Figure 3.8 shows a TEM micrograph of **(7)** which appears crystalline, whereas micrographs of **(4)** only showed amorphous material. Because the bridging between SMMs occurs along the Jahn-Teller axis, the bridging diamide chemically orders the sample, making it effectively "crystalline." The diameter of the wire is 0.9nm, which

agrees with the calculated MnO core size from XRD data of **(4)** [Lis80]. The ordering of wires into arrays is likely due to strong Van der Wals attraction between the wires as the solvent evaporates. EDAX data shows that the material is MnO and not crystalline impurity. The sample did not vaporize under the TEM, ruling out the possibility that the material was unpurified salt from the synthesis ($[KMnO_4]$ and $[Mn(CH_3O_2) \cdot 4H_2O]$).

The TEM micrograph of **(7)** also shows that the wires do not branch to form Y junctions, indicating that each SMM is bound to only one SMM on each side, even though there are two possible bridging sites at each end of one SMM. This can be explained either by steric hindrance, or by the fact that after one bond is formed between two SMMs, it is far more likely that a second bond will form between the two (by searching the conformational space) before another SMM links to the growing chain (i.e. the time scale of conformational search is shorter than the time scale of diffusion). The straightness of the wires would indicate that each SMM is bridged by two amides to each adjacent SMM, thereby limiting the conformational freedom.
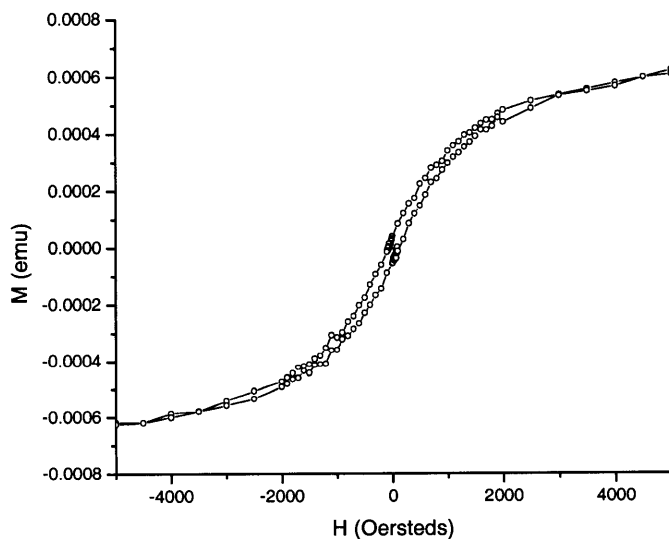
Figure 3.9 M-H curvesof Mn12-acetate molecular wires **(7)** showing room temperature hysteresis.

Figure 3.9 shows a room temperature M-H curve of the wires with no field-alignment. A small amount of hysteresis ($H_c = 72 Oe$) can be observed in figure 3.9, despite the fact that **(4)** is superparamagnetic. The hysteresis loop is narrower than the loop observed in field-aligned **(4)** ($H_c = 202 Oe$) (figure 3.2) because the SMMs in the chain are separated

61

by hexamethylene (C6) groups that decrease the (distance) dependent spin-interactions between the SMMs in the chain. M-H curves SMMs reacted with ethylene diamine (C2) and 1,12-aminododecane (C12) show no hysteresis. SMMs reacted with ethylene diamine are likely not bridged because the linker molecule is too short, and a wire cannot form. On the other hand, the C12 group is perhaps too long for significant spin interaction to occur between SMMs at room temperature.

The data above indicates the synthesis of a magnetic nanowire that is exactly one molecule wide and shows room temperature hysteresis. In the context of controlling biological molecules, the ability to bridge superparamagnets may allow a protein conformation to be altered, and permanently "turned off" by covalent locking. Observable hysteresis measurements would perhaps allow protein conformational changes to be monitored *in vivo* using a SQUID magnetometer.

Chapter 4: Wavelength Selective Photochemistry

4.0 – Introduction to wavelength selective photochemistry

This chapter proposes the design of a molecular assembly line based on wavelength selective photochemistry, in which the shuttle is covalently handed-off between monomer units much like ketides in a polyketide synthase. The basis of the system is the ability to use wavelength selective Norrish Type II photocleavage reactions of carbonyls to control the equilibrium of a Michael reaction (section 4.1). Experimental data on the ability to control this equilibrium will be shown, and potential backbones are proposed.

4.0.1 – Light-driven and programmable chemistries

Photochemical reactions are of great importance in organic, bioorganic, and polymer chemistries. Typically, UV irradiation is used as a means for polymerization initiation, intramolecular rearrangements, or photocleavage of protetcting groups or traceless linkers [Bochet02] [Kopecky92]. Largely driven by lab-on-chip gene arrays and solid-phase oligonucleotide synthesis, great efforts have been directed towards designing wavelength selective photocleavable chemistries for orthogonal protecting groups (figure 4.1) [Bochet02]. Although it is normally not a concern in protecting group chemistry, photocleavage reactions typically do not yield products that can be reacted to give back the initial molecule. This greatly limits the types of photochemical reactions that can be employed to build a molecular assembly line, which requires reversibility.
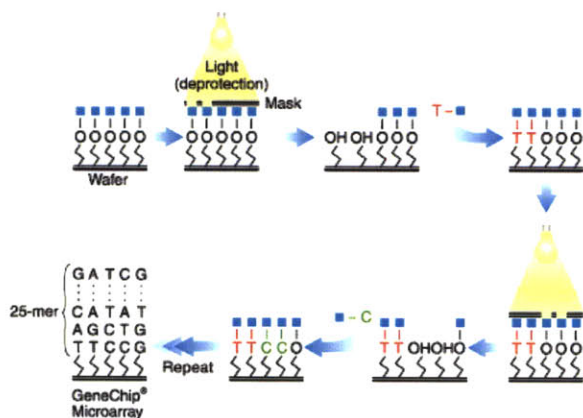
Figure 4.1 The role of photocleavable protecting groups in solid-phase DNA synthesis. The blue rectangles represent 5' photocleavable protecting groups necessary for making gene arrays on a chip by photolithography. Image from http://www.affymetrix.com.

However, such systems do exist, and have been demonstrated in the literature. In an extremely clever route towards reversible DNA ligation, Saito *et al.* ligated two DNA strands with a cyclobutane group formed by a light-driven 2+2 reaction with 5-vinyl-deoxyuridine (molecule 4 in figure 4.2a) at 366nm. Irradiating the DNA with 300nm light breaks the cyclobutane group and reverses the ligation step [Saito00]. Also, a class of charge-transfer complexes, called TCNQs (figure 4.2b), contains a large number of photochromic zwitterions with highly resolvable absorptions bands [Petty95]. These compounds could be used to build an assembly line based on electrostatic interactions between TCNQs and a charged shuttle.

a)
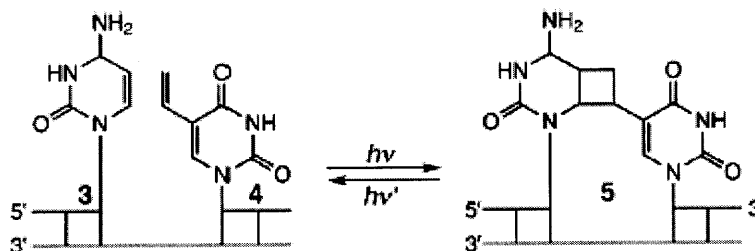
b)
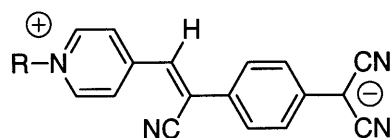
Figure 4.2 a) Reversible DNA ligation by light-driven "2+2" addition / photocleavage on a DNA backbone. Image from [Saito00]. **b)** Structure of a TCNQ photochromic zwitterion.

In truth, there are many routes towards building light-driven molecular machines and electronics (such as cis-trans isomerizations in azo-compounds and Förster resonance energy transfer, or FRET), but ultimately, the above-mentioned chemistries were not explored because of concerns over wavelength selectivity, or the fact that the shuttle/monomer interactions would not be covalent, since our goal here is to construct a purely synthetic analog of polyketide synthase that is capable of covalent hand-off.

4.0.2 – Molecular assembly line based on photochemistry

The reaction of choice for this embodiment of the molecular assembly line is the Norrish Type II photocleavage reaction of carbonyl compounds [Norrish38] [Norrish52]; the

Norrish Type II reaction results in an alkene and a terminal ketone or amide. Depending on their constituents, the photocleavage products may also be potential reactants for a base-catalyzed Michael reaction (figure 4.3a) [March92]. Therefore, the relative equilibrium of a Michael reaction can be controlled by UV light. Furthermore, the wavelengths at which the molecules (1-3) cleave are determined by and can be tuned by the R group. An alkyl ketone will cleave at λ = 280nm, whereas an aryl ketone and alkyl amide cleave at λ = 310nm and λ = 210nm, respectively. It is conceivable that a molecular assembly line could be constructed using this type of competitive Norrish/Michael reaction, as shown in figure 4.3b, where the Michael acceptor (4) is the shuttle and the Michael donor is the antenna. The experimental work in this chapter includes the photocleavage of an alkyl ketone and amide.

a)

where,

(1) R = alkyl (280nm)
(2) R = aromatic (310nm)
(3) R = NR'$_2$ (210nm)

b)
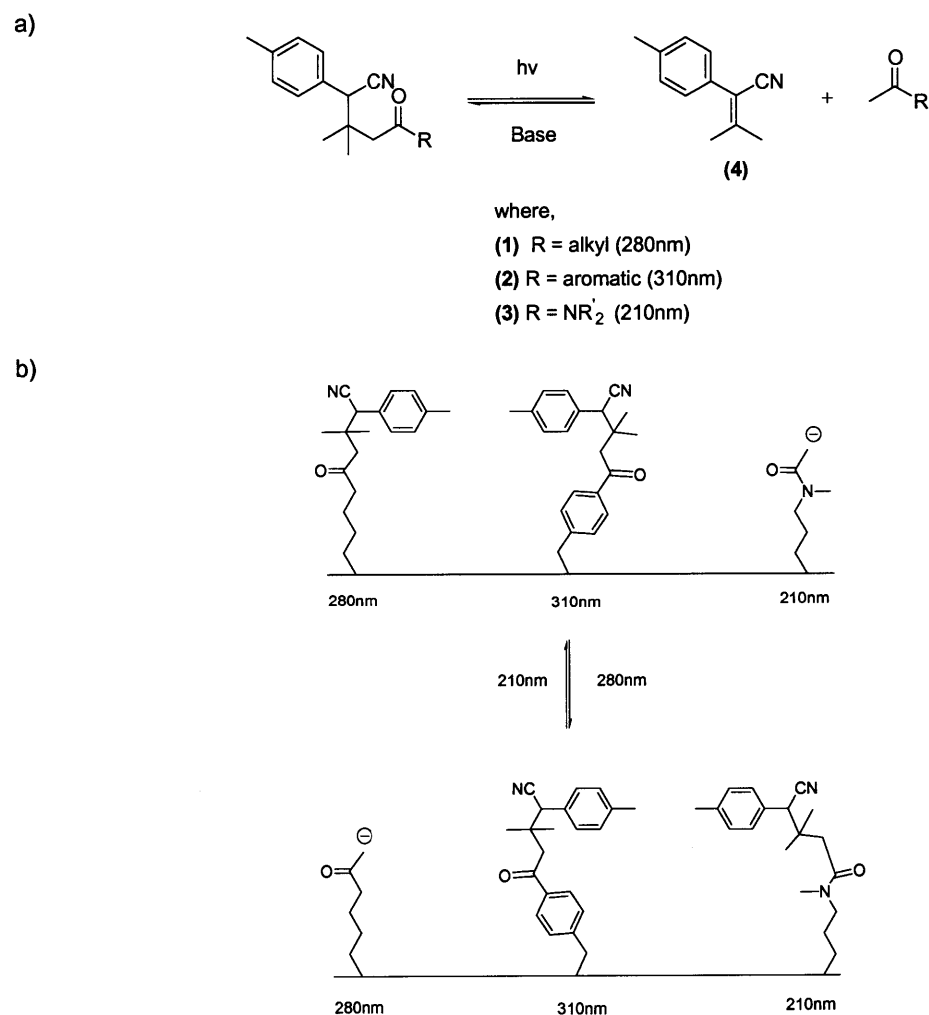
Figure 4.3 a) General reaction scheme for a Michael reaction in which the reaction equilibrium is driven by a competitive Norrish Type II photocleavage reaction. b) The repeating (1-2-3) unit of a molecular assembly line based on wavelength selective photocleavage of carbonyl compounds.

The general molecule was designed as it was for several reasons. First, the methyl groups at the γ-carbon sterically promote the Norrish Type II pathway for the photocleavage reaction, which could otherwise lead to the formation of an undesirable cyclobutane compound [Wagner83] by a Norrish Type I pathway. The p-tolyl group also favors the reaction taking a Norrish Type II pathway. Although it lowers the probability that the photocleavage reaction follows a Norrish Type II pathway versus a Norrish Type I pathway, the nitrile group makes (4) a far better electrophile and Michael acceptor.

It should be noted that the photocleavage of the o-tolyl version of (1) has been shown to be quantitative and yielded only the Norrish Type II products [Kim97]. The p-tolyl version is not as efficient because of the larger distance between the 1 and 4 carbons in the bi-radical intermediate, but as will be discussed in section 4.2, the reaction still only gave Norrish Type II products. The p-tolyl group was chosen over the o-tolyl group because of the availability of the reagent. A p-tolyl group was used instead of a benzene group to conserve the directing effects of having a substitution that would be required for linking the molecule to a solid-support.

One drawback of building a supramolecular molecular assembly line is the difficulty in synthesizing a linear backbone with reactive functionalities at exact, controlled locations... yet another reason to marvel at linear biological systems like poly-peptides and oligonucleotides. The most promising route is likely a ring-opening metathesis polymerization (ROMP), which is the route used in synthesizing the "endless" cyclic polymers reported by Grubbs et al. [Grubbs02] and the "universal polymer backbone" by Weck et al. [Weck03]. Many researchers have used DNA as a backbone for pre-programmed chemical reactions [Liu01] [Sheppard01], but the destructive nature of UV irradiation at wavelengths required for carbonyl photocleavage reactions makes DNA incompatible with the proposed chemistry.

Despite the difficulties in creating a backbone and limited applications in assembly given the destructive nature of UV irradiation, pursuing this avenue is extremely interesting for various reasons. A system with the ability to covalently hand-off a molecule would be a completely synthetic analog of the polyketide synthase. Wavelength selective photocleavable groups are extremely powerful as protecting groups. Furthermore, the

Michael reaction is a very general and useful reaction in organic chemistry, and the ability to drive the equilibrium of certain Michael reactions may prove useful, especially as the notions of *programmable chemistry* and *dynamic covalent chemistry* [Lehn99] [Stoddart02] become more and more prevalent.

4.1 – Experimental

All reagents were of the highest purity available and were used as received from Sigma-Aldrich unless otherwise indicated. Reactions under nitrogen were performed using standard techniques. ^{1}H-NMR spectra were taken on a Varian Unity 300MHz NMR spectrometer in $CDCl_3$. FTIR was taken using a Digi-Lab Excalibur FTS 3000 (neat, 64 scans, 4cm^{-1} resolution). HPLC chromatographs were obtained on a Varian Pro Star HPLC (monitored by UV absorption at 254nm).

Photocleavage reactions were performed under nitrogen in a photochemical micro-reaction assembly (Ace Glass model 7880) in cyclohexane (1mM) using a Pen-Rey 5.5W low-pressure mercury UV-lamp. (1) was irradiated with $\lambda > 290$nm by filtering lower wavelengths with borosilicate glass. (3) was irradiated with $\lambda \sim 215$nm by filtering with a 3 : 1 : 0.5 (v:v) mixture of ethanol : water : acetone with constant bubbling of nitrogen through the solution [Muel69]. HPLC of (1) and (3) were performed on a normal-phase silica column with 70:30 and 50:50 (v:v) heptane/THF as eluent, respectively.

The synthetic schemes for (1) and (3) are provided in figure 4.4.
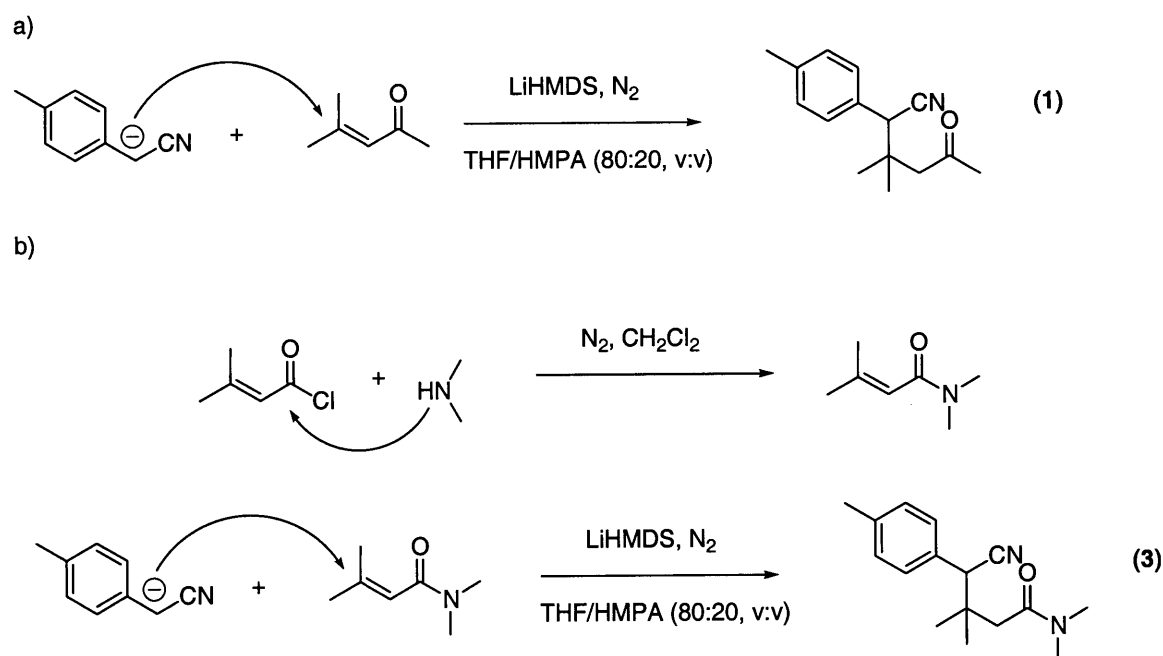
Figure 4.4 a) Synthetic scheme for 5-(p-tolyl)-5-cyano-4,4-dimethyl-2-pentanone (1). **b)** Synthetic scheme for 4-(p-tolyl)-4-cyano-3,3-dimethyl-N,N-dimethylbutaneamide (3).

Synthesis of 5-(p-tolyl)-5-cyano-4,4-dimethyl-2-pentanone **(1)**

660μL p-tolyl-acetonitrile (5mmol) and 572μL mesityl oxide were stirred in 50mL THF/HMPA (v:v 80:20) for 30 minutes at -78°C under nitrogen. 5mL of 1M LiHMDS in THF (5mmol) was added dropwise. The reaction was brought slowly to room temperature over 90 minutes, and stirred for two days at room temperature. The solution was extracted using ether / 1M HCl, and purified by silica gel flash chromatography (20:80 ethyl acetate/hexanes, v:v). After solvent removal by rotary evaporation, the sample was dried under high vacuum overnight. ^{1}H-NMR δ (ppm): 7.45-7.25 (4H, m), 4.82 (1H, s), 2.98 (3H, s), 2.36 (3H, s), 2.44-2.11 (2H, AB quartet), 1.25 (3H, s), 1.08 (3H, s). FTIR 2236 (m, s, CN), 1712.1 (s, br, CO).

Synthesis of 4-(p-tolyl)-4-cyano-3,3-dimethyl-N,N-dimethylbutaneamide **(3)**

557μL 3,3-dimethylacryloyl chloride (5mmol) and 6.25mL 2M dimethylamine in THF (2.5x, 12.5mmol) were stirred under nitrogen at 0°C for 30 minutes in 43.25mL CHCl$_2$. The compound was purified by extraction with ether / 1M HCl. Ether was removed by rotary evaporation to yield *3-methyl-N,N-dimethyl-2-buteneamide*.

5mL of 1M LiHMDS in THF (5mmol) was added dropwise to a solution of 660μL p-tolyl-acetonitrile (5mmol) in 25mL THF/HMPA (80:20, v:v), and stirred for 30 minutes at -78°C under nitrogen. 25mL of 0.2M 3-methyl-N,N-dimethyl-2-buteneamide in THF/HMPA was added dropwise. The reaction was brought slowly to room temperature over 90 minutes, and stirred for two days at room temperature. The solution was extracted using ether / 1M HCl, and purified by silica gel flash chromatography (70:30 ethyl acetate/hexanes, v:v). After solvent removal by rotary evaporation, the sample was dried under high vacuum overnight. ^{1}H-NMR: δ 7.26-7.12 (4H, m), 4.82 (1H, s), 2.97 (6H, s), 2.34 (3H, s), 2.43-2.11 (2H, AB quartet), 1.23 (3H, s), 1.05 (3H, s). FTIR (cm^{-1}) 2235 (m, s, CN), 1643 (s, br, CONR$_2$).

4.2 – Results and Discussion

Figure 4.5a and 4.5b show the respective HPLC chromatographs of **(1)** and **(3)** after 48 hours UV irradiation at $\lambda > 290$nm and $\lambda = 215$nm, respectively. In each chromatograph, the left peak represents the cleavage product / Michael acceptor, 3-(p-tolyl)-3-cyano-2-methyl-2-butene **(4)**, and the right peak represents the initial molecules **(1)** and **(3)** / Michael products. The Michael donors, acetone and N,N-dimethylacetamide, are not present in the spectra, as they are likely removed by water / heptane extraction during HPLC sample preparation. As expected, the cleavage reactions are wavelength selective as determined by thin-layer chromatography (TLC) analysis. Also as expected, the cleavage reaction followed a Norrish Type II pathway, and not a Type I cyclization, as determined by NMR analysis of products purified by silica-gel flash chromatography - **(4)** ^{1}H-NMR δ (ppm): 7.33-7.17 (4H, m), 2.38 (3H, s), 2.25 (3H, s), 1.92 (3H, s).
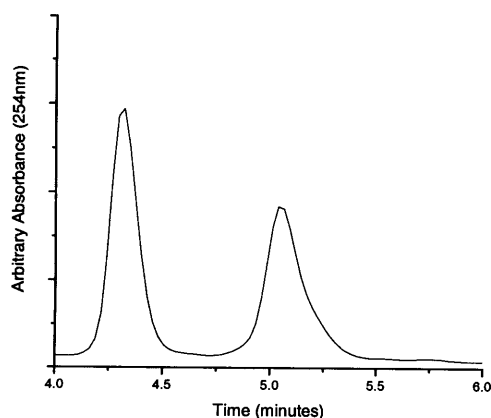
a) Compound **(1)** ($\lambda > 290$nm)   b) Compound **(3)** $\lambda = 215$nm
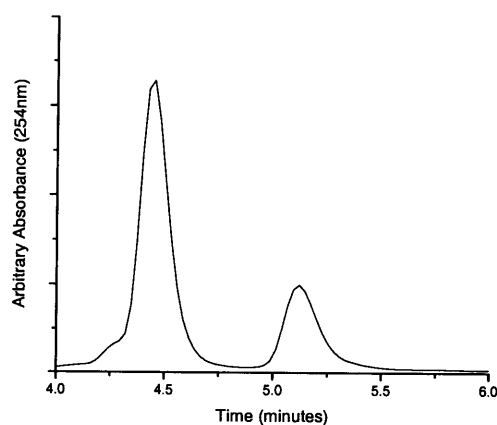
Figure 4.5 a) and b) HPLC chromatographs of **(1)** and **(3)** after 48 hours UV irradiation, respectively.

After 48 hours, the sample was aliquoted into two samples by removing half the sample volume from each reaction mixture, and an equimolar amount of LiHMDS was added to each sample. One aliquot was allowed to react in the presence of UV irradiation, and another was stirred under nitrogen in the dark at room temperature. After 48 hours, the relative equilibrium of the Michael reaction between **(4)** and the acetone enolate or the N,N-dimethylacetamide amidine was controlled by the UV irradiation, as shown in figure 4.6.

a) Compound **(1)**
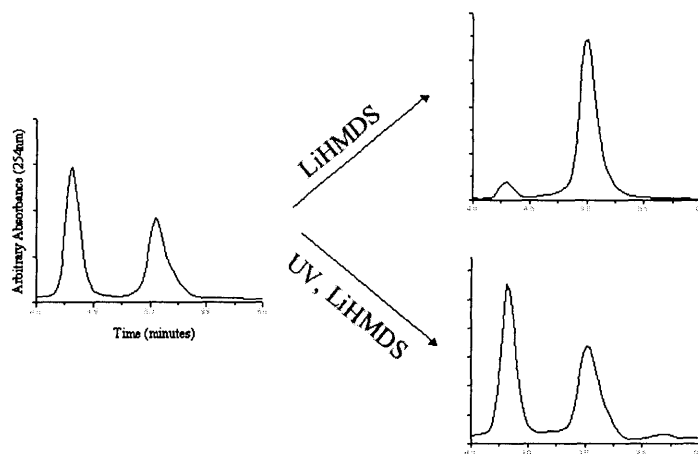
b) Compound **(3)**
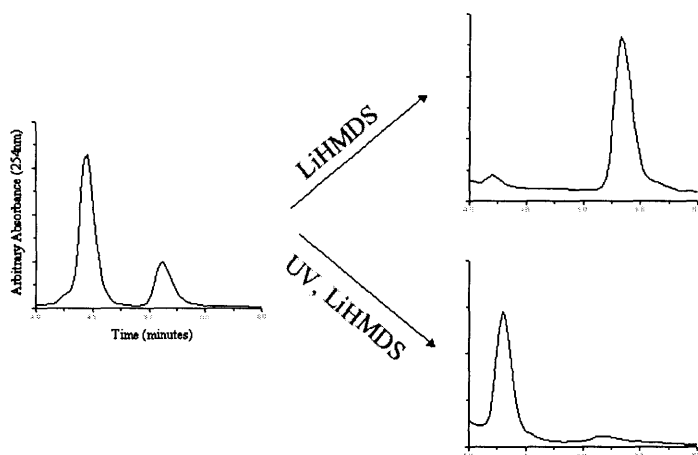
Figure 4.6 a) HPLC chromatographs of compound **(1)**. *Left,* after 48 hours irradiation at λ > 290nm only. *Right,* after 48 hours stirring in the presence of LiHMDS with and without UV irradiation. **b)** HPLC chromatographs of compound **(3)**. *Left,* after 48 hours irradiation at λ = 215nm only. *Right,* after 48 hours stirring in the presence of LiHMDS with and without UV irradiation

The basic principle of influencing the Michael reaction equilibrium has been proven, but the current experimental methods are limited in their ability to achieve quantitative yields of any product in the simultaneous presence of UV and lithium base. It is also impossible to make quantitative kinetic and thermodynamic comparisons between the compounds in the simultaneous presence of UV and lithium base. First, since the emission of the lamp is centered about 254nm, the number of photons in the experiment

is extremely low after wavelength filtering. Furthermore, the number of photons per unit time between the photocleavage reactions of **(1)** and **(3)** are not equal, making it difficult to compare the two. Second, in the case of compound **(1)**, the lithium base catalyzes the Aldol condensation of acetone, forming mesityl oxide; this prevents the Michael reaction from ever being quantitative. It could only be driven to quantitative yields in the presence of an excess of LiHMDS and acetone, and in the absence of UV irradiation. In the case of **(3)**, the N,N-dimethylacetamide amidine is a fairly poor nucleophile in comparison to an acetone enolate, changing the reaction kinetics between the two systems.

a)
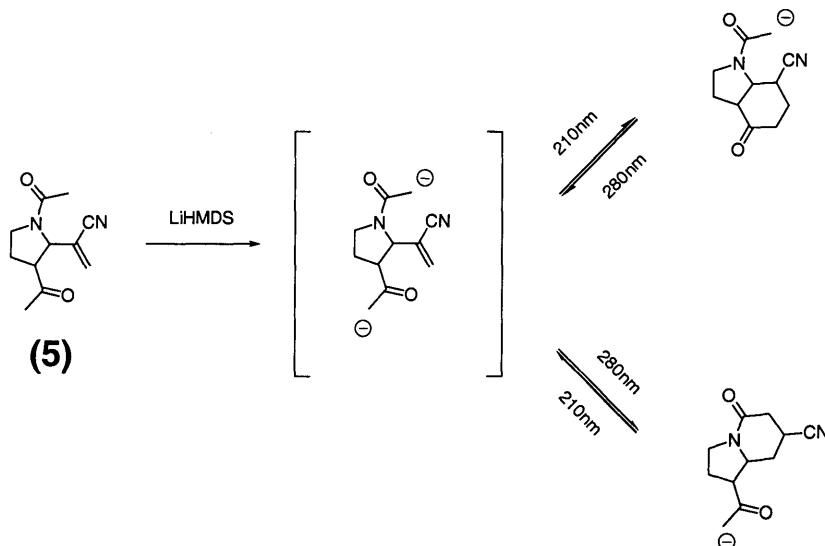
b)
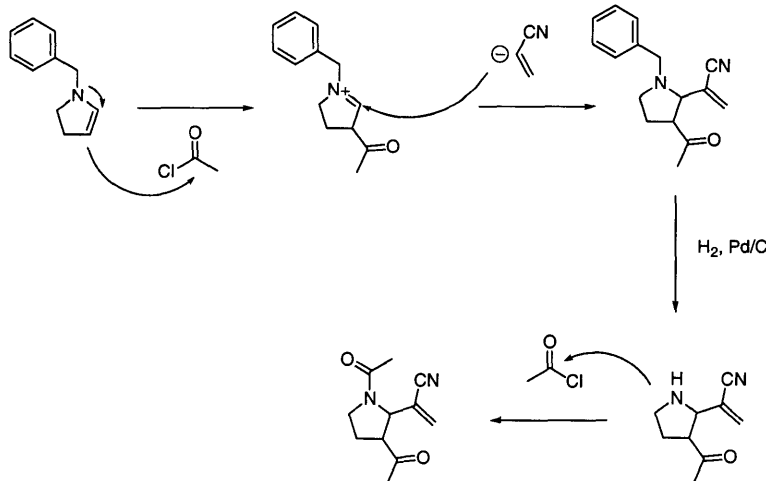
Figure 4.7 a) An intramolecular toggle switch driven by UV light. b) Potential synthetic scheme towards **(5)**.

Therefore, future experiments must first employ single-wavelength UV lasers with known powers or photon count per unit time. Second, the reactive functionalities – Michael acceptor, enolate, and amidine – must all be included in the same molecule so that the experimental time-scales are limited by the time-scale of bond-rotation, and not diffusion. This would prevent the formation of side-products like mesityl oxide and allow kinetic constants to be more easily determined. Figure 4.7 proposes a potential molecule to be synthesized in the future, an intramolecular toggle-switch (5); a potential synthetic scheme towards (5) [Mosley, UPR] is also given. The methyl groups that provide steric hindrance and the aromatic group that promotes hydrogen abstraction adjacent to the nitrile are not required. 3D-modeling (ChemDraw 3D Ultra, Cache) showed that products of the photoreaction following a Norrish Type I path, or a path via 1-5, 1-6, or 1-7 bi-radical intermediates, are unfavorable because of great ring strain.

Chapter 5: Summary and further work

While the "molecular assembly line" is, at this point, only a generalized scheme, the experimental results in this thesis have shown that its construction is within reason, as the basic requirement of the system as described in Chapter 1 - wavelength (or frequency) selective control over the interactions between monomeric antennae and a shuttle – has been met.

In the first approach, "RF Biology" (Chapter 2), an oligonucleotide was selectively dehybridized by coupling energy from 300MHz RFMF into covalently-attached 2.8nm cobalt nanoparticle antennae. In the future, the nanoparticle size distribution and the coupling chemistry to the oligonucleotides must be improved, and fluorescence measurements must be made with an internal thermometry standard in solution. Furthermore, a localized heating model has been proposed for the selective dehybridization of the oligonucleotide (as opposed to some mechanical resonance effect), but this has yet to be experimentally verified.

In the second approach, "Wavelength-selective photocleavage of carbonyl compounds" (Chapter 4), the equilibrium of a Michael reaction between an alkene acceptor and enolate or amidine donor was driven by UV irradiation at the absorption wavelength of the carbonyl bond in the resultant Michael product. This approach is particularly interesting because it holds the possibility of constructing a purely synthetic analog to the polyketide synthase in its ability to covalently "hand-off" small molecules. In the future, experiments must employ single-wavelength lasers, and a molecule must be synthesized that contains an alkene acceptor and both an enolate and amidine donor.

Upon the synthesis of a polymerized molecular assembly line, the issue of polymer chain coiling will have to be resolved. For example, the persistence length of double-stranded DNA is approximately 50nm [Bustamente00], and therefore, the length of a molecular assembly line built out of RF Biology parts will be limited to 50nm without employing external forces, like electric fields to align the phosphate backbone.

The experimental work in this thesis represent the most preliminary experimental steps towards constructing a molecular assembly line. In truth, the results are simple "proofs-

of-concept" that interactions between molecular components can be driven by external inputs, like RFMF and UV light, with wavelength/frequency selectivity. Until the synthesis of a fully polymerized molecular assembly line, the question will still remain whether the molecular assembly line is a useful construction, or whether its utility is merely as a "proof of concept."

Perhaps the most interesting outcomes will be the applications of the chemistries developed during the process but are outside the realm of building a molecular assembly line. For instance, the goal of controlling biological molecules so that they could be used as components in a molecular assembly line spawned the synthesis of molecular wires in Chapter 3 of this thesis. The ability to selectively break hydrogen bonds has great potential applications in biophysics and bioengineering, and the wavelength selective photocleavage reactions might have great potential applications in protecting group chemistry.

Only further experimental work can answer these questions, but given the initial set of results here, the outlook is promising.

Acknowledgements

First and foremost, I would like to thank my family for their undying support over the years… despite the fact that I can count the number of smart things that I've ever done on one hand.

***

I would also like to thank: *Joe Jacobson, Shuguang Zhang,* and *Bob O'Handley* for reading this thesis and providing valuable support throughout the process… all of the members of the *Molecular Machines* research group for creating a research environment full of free-flowing intellectual discussion and random acts of stupidity… *David Mosley* and *Kimberly Hamad-Schifferli* for their extreme patience and willingness to show me the ropes… *Mike Houlihan* for keeping the research group afloat… our collaborators in the *Zhang research group*… *Jason Taylor, Ben Recht,* and *Yael Maguire* for answering all the physics questions that I am too lazy to figure out on my own… *John D'Francesco* for valuable machining and design help… *Mike Frongillo* for taking "marvelous" TEM micrographs… *Alexander Rich* for generous use of his fluoremeter… *Richard Cook* and the staff at the MIT Biopolymers Lab for their expedient peptide synthesis and help in developing synthesis protocols… and finally, the past mentors who always went out of their way for me – *Jon Touster* and *Hongjie Dai* of Stanford University, *Janice Frazier* of IBM, and my high school chemistry teacher, *"Big" Paul Siler,* who showed me that chemistry is "cool stuff," and that it exists for some reason other than to make a student's life miserable.

***

<u>Molecular Machines</u>
<u>(Fall 2001 – Spring 2003)</u>

<u>Principal Investigator</u>
Joseph Jacobson

<u>Research scientist</u>
Peter Carr

<u>Post-doctoral fellows</u>
Kimberly Hamad-Schifferli
Kie-Moon Sung

<u>Graduate students</u>
Vikas Anant
Vikrant Agnihotri
Brian Chow
Will DelHagen
Sawyer Fuller
Saul Griffith
David Kong
David Mosley
Brent Ridley
Eric Wilhelm

<u>Staff</u>
Mike Houlihan
Murray Whitehead

From left to right: (bottom) Peter, Joe, and Kie-Moon *(middle)* Vikas, Eric, Will, and Brian *(top)* Dave M., Dave K., and Saul *(not shown):* Kim, Vikrant, Sawyer, Brent, Mike, and Murray.

References

[Alivisatos01]   Puntes, V.F.; Krishnan, K.M.; Alivisatos, P; Synthesis, self-assembly, and magnetic behavior of a two-dimensional superlattice of single-crystal ε-Co nanoparticles. *Appl. Phys. Lett.* 78, **2001**, 2187-2189

[Avouris01]   Derycke, V.; Martel, R.; Appenzeller, J.; Avouris, Ph.; Carbon Nanotube Inter- and Intramolecular Logic Gates. *Nano Lett.* 1, **2001**, 453-456

[Bacri00]   Roger, J.; Pons, J.M.; Masser, R.; Halbreich, A.; Bacri, J.C.; Some biomedical applications of ferrofluids. *Eur. Phys. J. AP.* 5, **1999**, 321-325.

[Belcher00]   Whaley, S.R.; English, D.S.; Hu, E.L.; Barbara, P.F.; Belcher, A.M.; Selection of peptides with semiconductor binding specificity for directed nanocrystal assembly. *Nature.* 405, **2000**, 665-668.

[Bochet02]   Bochet, C.G.; Photolabile protecting groups and linkers. *J. Chem. Soc. Perk. Trans. I.* 2, **2002**, 125-142.

[Brady92]   Cyr, J.L.; Brady S.T.; Molecular motors in axonal transport. Cellular and molecular biology of kinesin. *Mol. Neurobiol.* 6, **1992**, 137-155

[Bustamente00]   Bustamente, C.; Smith, S.B.; Liphardt, J.; Smith, D.; Single-molecule studies of DNA mechanics. *Curr. Opin. Struc. Biol.* 10, **2000**, 279-285.

[Campbell84]   Campbell, I.D.; Dwek, R.A.; *Biological Spectroscopy.* San Francisco, Benjamin/Cummings, **1984**.

[Carlson02]   Carlson, R.; The Pace and Proliferation of Biological Technologies. *Manuscript in preparation.* http://www.molsci.org.

[Christou01]   Artus, P.; Boskovic, C.; Yoo, J; Streib, W.E.; Brunnel, L.C.; Hendrickson, D.N.; Christou, G.; Single-Molecule Magnets: Site-Specific Ligand Abstraction from $[Mn_{12}O_{12}(O_2CR)_{16}(H_2O)_4]$ and the Preparation and Properties of $[Mn_{12}O_{12}(NO_3)_4(O_2CCH_2Bu^t)_{11}(H_2O)_4]$. *Inorg. Chem.* 40, **2001**, 4199-4210.

[Croqutte00]   Maier, B.; Strick, T.R.; Croquette, V.; Bensimon, D; Study of DNA Motors by Single Molecule Manipulation. *Single Mol.* 1, **2000**, 145-151.

[Dai01]   Kong, J.; Yenilmez, E.; Tombler, T.W.; Kim, W.; Dai, H.; Laughlin, R.B.; Liu, L.; Jayanthi, C.S.; Wu, S.Y.; Quantum Interference and Ballistic Transmission in Nanotube Electron Waveguides. *Phys. Rev. Lett.* 87, **2001**. 106801/1-106801/4

[DIMACS96]   Lipton, R.L.; Baum, E.B.; *DIMACS Workshop, April 4, 1995.* Providence, American Mathematical Society, **1996**.

[DOE02]   *Biomolecular Materials.* Report of the January 13-15, 2002 Conducted by the Basic Energy Sciences Advisory Committee to the Office of Science U.S. Department of Energy. http://www.sc.doe.gov/bes/besac/BiomolecularMaterialsReport.pdf

[Doyle02]   Csete, M.E.; Doyle, J.C.; Reverse Engineering of Biological Complexity. *Science.* 295, **2002**, 1664-1669.

[Dubertret01]   Dubertret, B.; Calame, M.; Libchaber, A.J.; Single-mismatch detection using gold-quenched fluorescent oligonucleotides. *Nature Biotech.* 19, **2001**, 365-370.

[Dumestre02]   Dumestre, F.; Chaudret, B.; Amiens, C.; Fromen, M.C.; Casanove, M.J.; Renaud, P.; Zurchar, P.; Shape Control of Thermodynamically Stable Cobalt Nanorods through Organometallic Chemistry. *Angew. Chem.* 114, **2002**, 4462-4465.

[Eigler93]   Eigler, D.M; Schweizer, E.K; Positioning single atoms with a scanning tunneling microscope. *Nature.* 324, **1990**, 524-526.

[Endow99]   Endow, S.A.; Determinants of molecular motor directionality. *Nature Cell. Biol.* 1, **1999**, E163-E167.

[Fannin99]   Fannin, P.C.; Perov, P.A.; Charles, S.W.; Complex susceptibility measurements of magnetic fluids over the frequency range 50MHz – 18GHz. *J. Phys. D: Appl. Phys.* 32, **1999**, 1583-1586.

[Fannin01]   Fannin, P.C.; Giannitsis, A.T.; Charles, S.W.; Frequency-dependent loss tangent and power factor of magnetic fluids. *J. Magn. Magn. Mat.* 226-230, **2001**, 1887-1889.

[Fannin02]   Fannin, P.C.; Slawska-Wanieskwa, A; Didukh, P.; Giannitsis, A.T.; Charles, S.W.; Dynamic properties of a system of cobalt nanoparticles. *Eur. Phys. J. AP.* 17, **2002**, 3-9.

[Feynman59]   Feynman, R.P.; There's Plenty of Room at the Bottom, *Caltech's "Engineering and Science."* **1959**. http://www.zyvex.com/nanotech/feynman.html

[Glick98]   Glick, B.R.; Pasternak, J.J.; *Molecular Biotechnology: Principles and Applications of Recombinant DNA, Second Edition.* Washington D.C., ASM Press, **1998**.

[Grubbs02]   Bielawski, C.W.; Benitez, D.; Grubbs, R.H.; An "Endless" Route to Cyclic Polymers. *Science.* 297, **2002**. 2041-2044.

[Hamad02]   Hamad-Schifferli, K.; Schwartz, J.J.; Santos, A.T.; Zhang, S;
                 Jacobson, J.M.; Remote electronic control of DNA hybridization
                 through inductive coupling to an attached metal nanocrystal antenna.
                 Nature. 415, **2002**, 152 – 155

[Hamad, UPR]   Hamad-Schifferli, K.; *unpublished result / personal communication.*
                 Current location – MIT Department of Mechanical Engineering.

[Hergt98]   Hergt, R; Wilfried, A.; d'Ambly, C.G.; Hilger, I.; Kaiser, W.A.; Richter,
                 U.; Schmidt, H.G.; Physical Limits of Magnetic Fluid Hyperthermia.
                 IEEE Trans. Magn. 34, **1998**, 3745-3654.

[Herz02]   Herz, L.M.; Phillips, R.T.; Fine Lines from Dots. *Nature Mat.* 1, **2002**,
                 212-213.

[Hopfield89]   Hopfield, J.J.; Onuchic, J.N.; Beratan, D.N.; Electronic Shift Register
                 Memory Based on Molecular Electron Transfer Reactions. *J. Phys.
                 Chem.* 93, **1989**, 6350-6357.

[Hopwood97]   Hopwood, D.A.; Genetic Contributions to Understanding Polyketide
                 Synthases. *Chem. Rev.* 97, **1997**, 2465-2497.

[Kim97]   Kim, T.Y.; Ko, E.S.; Park, B.S.; Yoon, H.; Chae, W.K.;
                 Photochemistry of 5-(o-tolyl)-5-cyano-4,4-dimethyl-2-pentanone.
                 Bull. Korean. Chem. Soc. 18, **1997**, 439-441.

[Komiyama99]   Asanuma, H.; Yoshida, T.; Ito, T.; Komiyama, M.; Photo-responsive
                 oligonucleotides carrying azo-benzene at the 2'-position of uridine.
                 Tet. Lett. 40, **1999**, 7995-7998.

[Kopecky92]   Kopecky, J.; *Organic Photochemistry: A Visual Approach.* New York:
                 VCH, **1992**.

[Lehn99]   Lehn, J.M.; Dynamic Combinatorial Chemistry and Virtual
                 Combinatorial Libraries. *Chem. Eur. J.* 5, **1999**, 2455-2463.

[Lehn00]   Lehn, J.M.; Programmed Chemical Systems: Multiple Subprograms
                 and Multiple Processing/Expression of Molecular Information.
                 Chem. Eur. J. 6, **2000**, 2097-2102.

[Lis80]   Lis, T.; Preparation, structure, and magnetic properties of a
                 dodecanuclear mixed-valence manganese carboxylate. *Acta Cryst.
                 B*; B36, **1980**, 2042-6.

[March92]   March. J.; *Advanced Organic Chemistry: Reacions, Mechanisms,
                 and Structure, Fourth Ed.* New York: John Wiley & Sons, **1992**.

[McEuen96]   Dixon, D; Kouwenhoven, L.P.; McEuen, P.L.; Nagamune, Y.;
                Motohisa, J.; Sakaki, H.; Influence of energy level alignment on
                tunneling between coupled quantum dots. *Phys. Rev. B.*, 53, **1996**,
                12625-12628.

[Mosley, UPR]   Mosley, D.W.; *unpublished result / personal communication*. Current
                location – MIT Media Laboratory.

[Muel69]   Muel, B.; Malpiece, C.; Chemical filters for narrow band U.V.
                irradiation between 235-300nm. *Photochem. Photobiol.* 10, **1969**,
                283-291.

[Murray99]   Murray, C.B.; Sun, S.; Synthesis of monodisperse cobalt
                nanocrystals and their assembly into magnetic superlattices (invited)
                J. Appl. Phys. 85, **1999**, 4325-4330.

[Nakamoto68]   Kedzia, B.B.; Armendarez, P.X.; Nakamoto, K.; Infra-red spectra and
                normal co-ordinate analyses of metal biuret complexes. *J. Inorg.
                Nucl. Chem.* 30, **1968**, 849-860.

[Narumi00]   Kitayama, S.; Narumi, I.; Kikuchi M.; Watanabe. H; Mutation in recR
                gene of *Deinococcus radiodurans* and possible involvement of its
                product in the repair of DNA interstrand cross-links. *Mut. Res.* 461,
                2000, 179-187.

[Norrish38]   Bamford, C.H.; Norrish, R.G.W; Primary Photochemical Reactions.
                Part XI. The photolysis of Aldehydes and Ketones in Paraffinoid
                Solution. *J. Chem. Soc.* **1938**, 1531-1543.

[Norrish52]   Booth, G.H.; Norrish, R.G.W.; Photochemical Studies of Some
                Organic Nitrogen Derivatives. *J. Chem. Soc.* **1952,** 188-198

[Nuss97]   Woolard, D.L.; Koscica, T.; Rhodes, D.L.; Cui, H.L.; Pastore, R.A.;
                Jensen, J.O.; Jensen, J.L.; Loerop, W.R.; Jacobsen, R.H.; Mittleman,
                D.M.; Nuss, M.C.; Millimeter Wave-induced Vibrational Modes in
                DNA as a Possible Alternative to Animal Tests to Probe
                Carcinogenic Mutations. *J. Appl. Toxic.* 17, **1997**, 243-246.

[O'Handley00]   O'Handley, R.C.; *Modern Magnetic Materials. Principles and
                Applications*. New York, John Wiley & Sons, **2000**.

[Petty95]   Petty, M.C.; Bryce, M.R.; Bloor, D.; *An Introduction to Molecular
                Electronics*. London, Edward Arnold, **1995**.

[Rosensweig02] Rosenzweig. R.; Heating magnetic fluid with alternating magnetic
                field. *J. Magn. Magn. Mat.* 252, **2002**, 370-374.

[Saito00]   Fujimoto, K.; Matsuda, S.; Saito, I.; Template-Directed
                 Photoreversible Ligation of Deoxyoligonucleotides via 5-
                 Vinyldeoxyuridine. *J. Am. Chem. Soc.* 122, **2000**, 5646-5647.

[Sessoli93]   Sessoli, R.; Tsai, H.; Schake, A.; Wang, S.; Vincent, J.; Folting, K.;
                 Gatteschi, D.; Christou, G.; Hendrickson. D.; High-spin molecules:
                 [$Mn_{12}O_{12}(O_2CR)_{16}(H_2O)_4$]. *J. Am. Chem. Soc.* 115, **1993**, 1804-1816.

[Sharp00]   Sharp, D.J.; Rogers, G.C.; Scholey, J.M.; Microtubule motors in
                 mitosis. *Nature.* 47, **2000**. 41-47.

[Simpson98]   Hitchman, T.S.; Crosby, J.; Byrom, K.J.; Cox, R.J.; Simpson, T.J.;
                 Catalytic self-acylation of type II polyketide synthase acyl carrier
                 proteins. *Chem. Biol.* 5, **1998**, 35-47.

[Stoddart01]   Barbera, P.F.; Stoddart, J.F.; *Accounts of Chemical Research:*
                 Molecular Machines Special Issue, 34, **2001**, 409-522

[Stoddart02]   Rowan, S.J.; Cantrill, S.J.; Cousins, G.R.L.; Sanders, J.K.M.;
                 Stoddart, J.F.; Dynamic covalent chemistry. *Angew. Chem. Int. Ed.*
                 41, **2002**, 899-952.

[Sung, UPR]   Sung, K.M.; *unpublished result / personal communication.* Current
                 location – MIT Media Laboratory.

[Thompson98]   Thompson. M.T.; Simple Models and Measurements of Magnetically
                 Induced Heating Effects in Ferromagnetic Fluids. *IEEE Trans. Magn.*
                 34, **1998**, 3755-3764

[Vale00]   Vale, R.D.; Milligan, R.A.; The Way Things Move: Looking Under the
                 Hoods of Molecular Motor Proteins. *Science.* 288, **2000**, 88-95.

[Vogel01]   Hess, H.; Clemmens, J.; Qin, D.; Howard, J.; Vogel. V.; Light-
                 Controlled Molecular Shuttles Made from Motor Proteins Carrying
                 Cargo on Engineered Surfaces. *Nano Lett..* 1, **2001**, 235-239.

[Wagner83]   Wagner, P.J.; Conformational Flexibility and Photochemistry. *Acc.*
                 Chem. Res. 16, **1983**, 461-467.

[Walsh01]   Walsh, C.T.; Chen, H.; Keating, T.A.; Hubbard, B.K.; Losey, H.C.;
                 Luo, L.; Marshall, C.G.; Miller, D.A.; Patel, H.M.; Tailoring enzymes
                 that modify nonribosomal peptides during and after chain elongation
                 on NRPS assembly lines. *Curr. Opin. Chem. Biol.* 5, **2001**, 525-534.

[Weck03]   Weck, M.; Stubbs, L.P.; Towards a Universal Polymer Backbone:
                 Design and Synthesis of Polymeric Scaffold Containing Terminal
                 Hydrogen-Bonding Recognition Motifs at Each Repeating Units.
                 Chem. Eur. J. 9, **2002**, 992-999.

[Whitesides02]   Boncheva, M.; Gracias, D.H.; Jacobs, H.O.; Whitesides, G.M.; Biomimetic self-assembly of a functional assymetrical electronic device. *PNAS*. 99, **2002**, 4937-4940.

[Winfree96]   Winfree, E.; On the computational power of DNA annealing and ligation. In [DIMACS96]. 199-221.